



**NIST Grant/Contractor Report
NIST GCR 24-055**

InSAR Analysis over the Eastern Coastline of Florida

TRE Altamira, Inc.
Exponent, Inc.

This publication is available free of charge from:
<https://doi.org/10.6028/NIST.GCR.24-055>

**NIST Grant/Contractor Report
NIST GCR 24-055**

**InSAR Analysis over the Eastern
Coastline of Florida**

TRE Altamira, Inc.
Exponent, Inc.

This publication is available free of charge from:
<https://doi.org/10.6028/NIST.GCR.24-055>

August 2024



U.S. Department of Commerce
Gina M. Raimondo, Secretary

National Institute of Standards and Technology
Laurie E. Locascio, NIST Director and Under Secretary of Commerce for Standards and Technology

Certain equipment, instruments, software, or materials, commercial or non-commercial, are identified in this paper in order to specify the experimental procedure adequately. Such identification does not imply recommendation or endorsement of any product or service by NIST, nor does it imply that the materials or equipment identified are necessarily the best available for the purpose.

This publication was produced as part of contract 1333ND23PNB730071 with the National Institute of Standards and Technology. The contents of this publication do not necessarily reflect the views or policies of the National Institute of Standards and Technology or the US Government.

NIST Technical Series Policies

[Copyright, Use, and Licensing Statements](#)

[NIST Technical Series Publication Identifier Syntax](#)

Publication History

Approved by the NIST Editorial Review Board on 2024-08-23

How to Cite this NIST Technical Series Publication

TRE Altamira, Inc. and Exponent, Inc. (2024) InSAR Analysis over the Eastern Coastline of Florida. (National Institute of Standards and Technology, Gaithersburg, MD), NIST GCR 24-055. <https://doi.org/10.6028/NIST.GCR.24-055>

Executive Summary

The National Institute of Standards and Technology (NIST) contracted TRE ALTAMIRA (TREA) for a historical Interferometric Synthetic Aperture Radar (InSAR) analysis to produce surface displacement measurements over a wide Area Of Interest (AOI) of approximately 709.6 square miles (1,838 km²) along the eastern coastline of Florida. The main scope of the study was to identify potential regional displacement trends affecting the area.

TREA processed historical Sentinel-1 (SNT) imagery available over the AOI up to the end of January 2023, using its proprietary SqueeSAR® algorithm. Transects specifically required by NIST were also generated and attached to this document in Appendix 1.

The current document constitutes the final Technical Report and includes a detailed description of the imagery (Section 2), an introduction to InSAR technology (Section 3), an overview of the SqueeSAR results obtained (Section 4), and the findings of the data analysis and interpretation (Section 5), which aimed to characterize and quantify observed trends in ground surface displacement across the AOI. The analysis and interpretation of the InSAR results was performed in collaboration with Exponent, Inc. (EX). This effort included “ground truthing” of the InSAR time series, identification of potential sources of error, and the documentation and evaluation of observed spatial and temporal data trends in the context of geological, hydrological, and anthropogenic conditions (primarily construction related).

Summary of imagery and InSAR Processing:

- The InSAR analysis used historical low-resolution SNT imagery (5m x 20 m pixel size) available over the site, consisting of 177 images acquired between September 2016 and January 2023 in the ascending orbit.
- The SqueeSAR processing of the historical imagery produced full resolution measurements in the form of point clouds.
- Each measurement point (MP) contains a time series of displacement (i.e., cumulative displacement with respect to the first radar image of the data stack), the average displacement rate and acceleration over the period of the analysis, and quality parameters.
- All measurements provided by this study are 1-D Line Of Sight (LOS) measurements because of the absence of historical data acquired over the site in double orbit (i.e., ascending and descending) in overlapping periods.

Summary of Data Quality Analysis:

- The quality of the InSAR results was evaluated based on the stability of the reference point by “ground truthing” the data against absolute GPS displacement measurements and then interpreted in the context of processes observed from the acquired available ancillary data (tidal data, ground monitoring data and historical aerial photos).
- The reference point was located in a stable area with no visible ground changes during the period of study, and measurement point time series in the areas surrounding permanent GPS stations reflected similar trends in relative ground displacement.
- “Ground truthing” of the InSAR time series confirms that the data was reliable for characterizing relative ground displacement trends.
- Possible sources of error were highlighted and discussed to support the Data Analysis. In particular, the interpretation of spatial and temporal trends should consider the limitations of InSAR technology, including the constraints imposed by the resolution of the satellite imagery, the frequency of the acquisitions and the precision of the measurements.
- Measuring displacements that are smaller than the resolution of the satellite (i.e. 20x5 m pixel size for SNT) is not possible. If the movement involves one single pixel (i.e., one single measurement point) it is only possible to correctly measure a displacement within one quarter of the wavelength ($\pm\lambda/4$) between two consecutive images, which is ± 1.4 mm using C-band SNT data. Rapid movements (i.e., larger than this theoretical limit) can be detected if the deforming area involves at least a few pixels or a cluster of measurement points.
- Single jumps in the displacement time series (i.e., a displacement step without a subsequent trend change involving at least 4 to 5 consecutive images) may be the effect of residual atmospheric or decorrelation noise in the time series. Similarly, displacement jumps and minimal trend changes within the error bar of the measurements are deemed not statistically relevant.
- Measurement point location accuracy using low-resolution SNT imagery is in the order of ± 8 m in the NS direction, ± 12 m in the EW direction and ± 8 m in the vertical direction. For this reason, SNT data is not generally used for the analysis of small single buildings or residential structures that are the size of a few pixels.
- It is noted that interpreting 1-D Line Of Sight (LOS) displacement as vertical displacement requires the assumption of negligible horizontal components of the real displacement vector. If this assumption is not verified, the vertical estimation can be affected by a bias.

Summary of Data Analysis and Conclusions:

- The analysis of the SNT results over the AOI included the transects defined by NIST, displacement, acceleration and seasonality maps. The analysis confirms that there is no evidence of wide-area subsidence, acceleration or seasonal trends affecting the area.
- However, localized areas of displacement in the study area can be identified in the InSAR results by looking at clusters of points with a displacement rate greater than the precision of the measurements and/or non-linear trends. Examples of localized areas of displacement are provided in this report but their investigation was not part of the scope of this study. Additional site-specific investigations would be required to confirm the trends identified in the InSAR data and verify the possible sources of surface displacement.

Table of Contents

Executive Summary	3
Acronyms and Abbreviations	8
References	9
1. Introduction	11
2. Radar Data	13
3. InSAR technology	16
3.1. SAR Interferometry – Basic principle	16
3.2. SqueeSAR	18
3.2.1. 1-D LOS measurements	19
3.2.2. Measurement precision and sources of inaccuracy	21
4. Results	26
4.1. Overview	26
5. Data Analysis	31
5.1. Summary of Ancillary Data	33
5.1.1. Historical GNSS Data	33
5.1.2. Historical Tidal Data	35
5.1.3. Historical Groundwater Monitoring Data	35
5.1.4. Historical Subsurface Geological Data	36
5.1.5. Historical Aerial Photos	37
5.2. Evaluation of the InSAR data and sources of errors	37
5.2.1. Evaluation of the REF point	38
5.2.2. Potential Sources of Error	48
5.3. Analysis of displacement trends	49
5.3.1. Localized ground settlement	51
5.3.2. Ground settlement associated with anthropogenic fill	53



5.3.3.	Ground settlement due to coastal development	55
5.3.4.	Coastal subsidence associated with changed conditions	57
6.	Conclusions.....	59
7.	Appendix 1: Transects	60
7.1.	Local-SNT – T1.....	61
7.2.	Local-SNT – T2.....	62
7.3.	Local-SNT – T3.....	63
7.4.	Local-SNT – T4.....	64
7.5.	Local-SNT – T5.....	65
7.6.	Local-SNT – TA	66
7.7.	Local-SNT – TB.....	67
7.8.	Local-SNT – TC.....	68
7.9.	Local-SNT – TD	69
7.10.	Local-SNT – TE.....	70

Acronyms and Abbreviations

AOI	Area of Interest
ATS	Average Time Series
AZ	Azimuth satellite direction
DEM	Digital Elevation Model
DInSAR	Differential SAR Interferometry
DTM	Digital Terrain Model
EX	Exponent, Inc.
GIS	Geographic Information System
GNSS	Global Navigation Satellite System
InSAR	Interferometric Synthetic Aperture Radar
LOS	Line of Sight
MP	Measurement Point
NIST	National Institute of Standards and Technology
PSInSAR™	Permanent Scatterers SAR Interferometry technique
REF	Reference point
RG	Range satellite direction
SAR	Synthetic Aperture Radar
SNT	Sentinel Satellite
SqueeSAR®	The most recent InSAR algorithm patented by TREA
TREA	TRE Altamira Inc.
TS	Time Series

References

- Berardino, P., Fornaro, G., Lanari, R. and Sansosti, E. (2002) A New Algorithm for Surface Deformation Monitoring Based on Small Baseline Differential SAR Interferograms. *IEEE Transactions on Geoscience and Remote Sensing*, 40(11), 2375–2383.
- Blewitt, G., & Hammond, W. (2018). Harnessing the GPS data explosion for interdisciplinary science. *Eos*, 99
- Bürgmann, R., Rosen, P.A. and Fielding, E.J. (2000) Synthetic Aperture Radar Interferometry to Measure Earth's Surface Topography and Its Deformation. *Annual Review of Earth and Planetary Sciences*, 28, 169–209.
- Cherkassky, V., Mulier, F., Vapnik, V. (1996) Comparison of VC-method with classical methods for model selection, *Proc. 1996 World Congress on Neural Networks*.
- Duncan J., 1993, Geologic Map of Dade County Florida, *Open-File Map Series 67*, Florida Geological Survey, Department of Natural Resources, Map.
- Ferretti, A. (2014) Satellite InSAR Data: reservoir monitoring from space. *Earthdoc, (EET 9)*, 156 pp.
- Ferretti, A., Fumagalli, A., Novali, F., Prati, C., Rocca, F. and Rucci, A. (2011) A new algorithm for processing interferometric data-stacks: SqueeSAR. *IEEE Transactions on Geoscience and Remote Sensing*, 49(9), 3460–3470
- Ferretti, A., Prati, C. and Rocca, F. (2001) Permanent Scatterers in SAR Interferometry. *IEEE Transactions on Geoscience and Remote Sensing*, 39(1), 8–20.
- Geologic Well and Borehole Data Map*, Map Direct, Florida Geological Survey, Florida Department of Environmental Protection, <https://ca.dep.state.fl.us/mapdirect/?webmap=158cbdbaeb6245438e5e7be30368f7e8>
- Massonnet, D. and Feigl, K.L. (1998) Radar Interferometry and Its Application to Changes in the Earth's surface. *Reviews of Geophysics*, 36(4), 441–500.
- Matson, G.C., and Clapp, F.G., 1909, A preliminary report on the geology of Florida with special reference to the stratigraphy, Florida Geological Survey, *Annual Report no. 2*, p13-173
- Matson, G.C., and Clapp, F.G., Sanford, S., 1909, *Geologic and Topographic Map of Florida*, Prepared by the United States Geological Survey, Map.
- Rocca, F., Prati, C. and Ferretti, A. (1997) An overview of ERS-SAR interferometry. *3rd ERS Symposium, Space at the Service of Our Environment*, Florence, 17–21 March, 1997, ESA-SP- 414, Vol 1, xxvii– xxxvi,

<http://earth.esa.int/workshops/ers97/program-details/speeches/rocca-et-al/>. Sanford, S., Topography and Geology of Southern Florida, Florida Geological Survey, *Annual Report no. 2*, p.177-231

Scott, T.M., Campbell, K.M., Rupert, F.R., Arthur, J.D., Missimer, T.M., Lloyd, J.M., Yon, J.W., and Duncan, J.G., 2001, *Geologic Map of the State of Florida*, Florida Geological Survey & Florida Department of Environmental Protection, Map Series 146, scale 1:750,000. Revised 2006

Scott, Thomas M.P.G. #99, Text to Accompany the Geologic Map of Florida, *Open-file Report 80*, Florida Geological Survey, 2001.

Web sources:

Geologic units in Miami-Dade County, Florida at <https://mrdata.usgs.gov/geology/state/fips-unit.php?code=f12086>

Nevada Geodetic Laboratory: <http://geodesy.unr.edu/>

NOAA: <https://www.ncei.noaa.gov/access>

Shuttle Radar Topography Mission (SRTM): <https://www2.jpl.nasa.gov/srtm/>

USGS: <https://www.usgs.gov/>

1. Introduction

TRE Altamira Inc. (TREA) was contracted by the National Institute of Standards and Technology (NIST) to perform an InSAR analysis of ground displacement over the eastern coastline of Florida, by using TREA’s patented SqueeSAR® technique and Sentinel-1 (SNT) radar satellite imagery covering the period September 2016 - January 2023.

The Area of Interest (AOI) for this analysis was defined by NIST (coordinates reported in Table 1) and covers approximately 709.6 square miles (1,838 km²) along the eastern coastline of Florida (Figure 1).

The objectives of the analysis were the following:

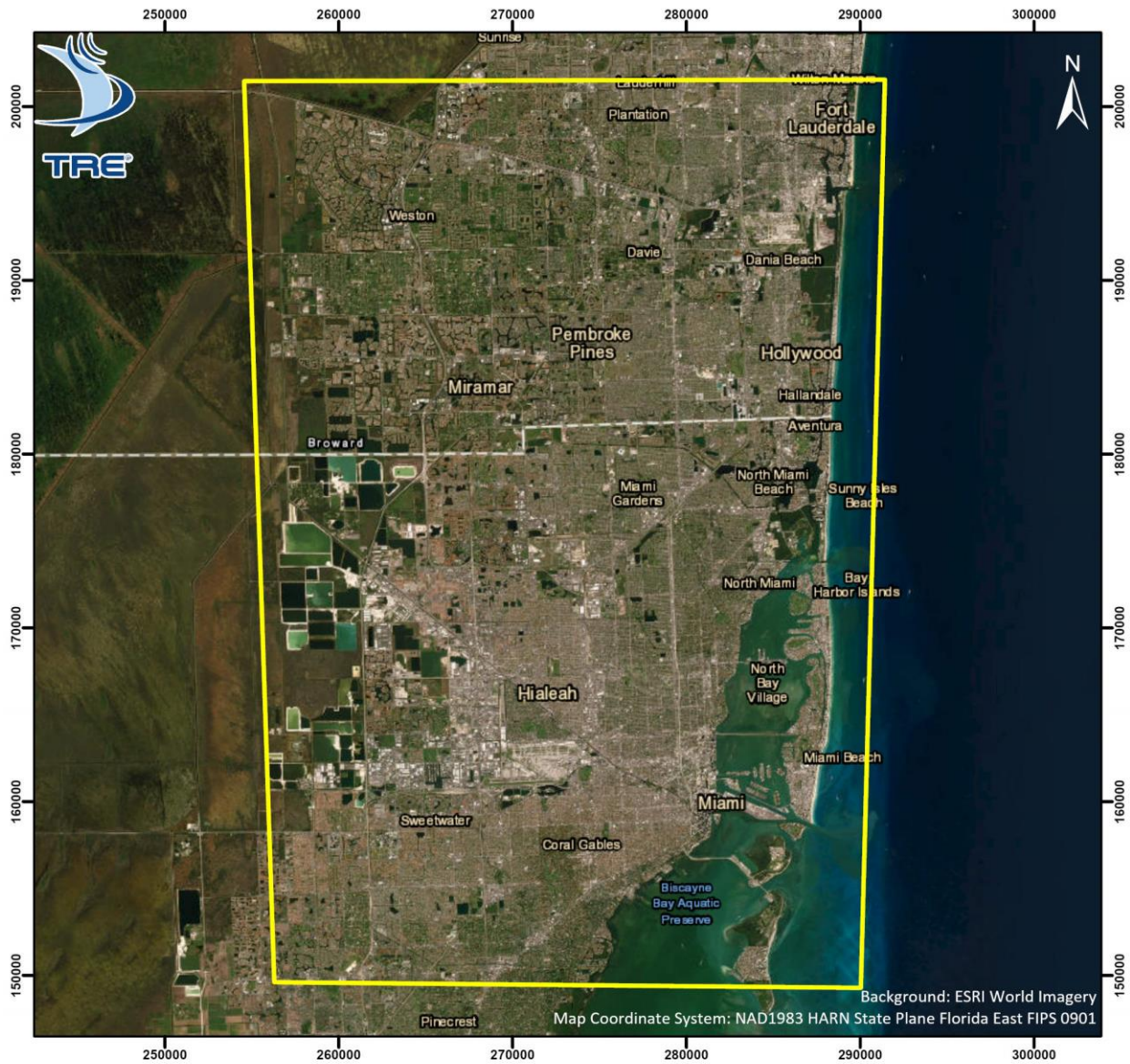
- Provide NIST with historical InSAR measurements to evaluate surface displacement trends over the area.
- Provide transects and point time series to support NIST in visualizing changes in the surface displacement measurements over time.
- Data analysis and interpretation to evaluate the results and draw interpretations of the displacement trends.

The analysis and interpretation of the InSAR results has been performed by TREA in collaboration with Exponent Inc. (EX).

The current document constitutes the Technical Report and includes details about the satellite imagery acquired (Section 2), an overview of InSAR technology (Section 3), the results obtained (Section 4), the findings of the data analysis (Section 5) and final conclusions (Section 6). The transects requested by NIST are included in Appendix 1.

Table 1: Bounding Box Coordinates (Latitude and Longitude) for the AOI.

Coordinates	North	South	East	West
AOI	26° 8'41.11"N	25°41'12.30"N	80° 6'27.98"W	80°26'24.59"W



 Area Of Interest (AOI)



Figure 1: Area of interest (AOI).

2. Radar Data

The analysis used historical imagery collected by the satellite Sentinel-1 (SNT) over the AOI, consisting of 177 SAR images collected from an ascending orbit between 27 September 2016 and 30 January 2023. Table 2 and Table 3 provide an overview of the main characteristics of the satellite, the imagery processed and the satellite's specific orbital parameters over the area of interest. The imagery temporal distribution is shown in Figure 2.

SAR satellites follow sun-synchronous orbits that are slightly inclined with respect to the meridians, and illuminate a land strip, or swath, of up to 250 km in width by 200 km in length for SNT. The direction parallel to a satellite's flight path is called the azimuth ("AZ"), which is slightly inclined with respect to the North-South direction (angle δ in Table 3). The sensor to target direction is orthogonal to the orbit and the distance from the satellite along this direction is called the slant range ("range") or Line of Sight ("LOS") distance. The LOS is inclined by an off-nadir angle (angle θ in Table 3) with respect to the vertical axis. The orientation of the LOS with respect to the North-South (N), East-West (E) and Height (H) directions is described by the LOS versors in Table 3.

Due to the combination of Earth's rotation with the sun-synchronous satellite orbits, an area on the ground surface can be imaged by a satellite as it travels both along a North-to-South (descending orbit) flight path and South-to-North (ascending orbit) flight path (Figure 3). The historical imagery available over the AOI for this analysis was collected from an ascending orbit.

InSAR measures the projection of the real vector of displacement onto the satellite LOS and provides one-dimensional measurements of satellite-to-target range changes along the LOS; positive values correspond to movement toward the satellite, while negative values correspond to movement away from the satellite. Hence, InSAR measurements indicate movement along a specific LOS direction of the satellite and not in the vertical direction (i.e., not perpendicular to the ground surface). Further details and discussion on the assumptions required when using LOS measurements as vertical measurements are provided in Section 3.2.1.

Table 2: Radar data characteristics

Satellite	Band	Wavelength	Pixel Resolution (Range x Azimuth)	Revisit frequency
SNT	C-band	5.6 cm	5 m x 20 m	12 days

Table 3: Orbital parameters of the imagery used for the current study.

Orbit	Data range	# images	LOS Angle (Θ)	LOS Angle (δ)	LOS Versors		
					N	E	H
Ascending	27 Sept 2016 – 30 Jan 2023	177	42.2°	10.6°	-0.124	-0.66	0.741

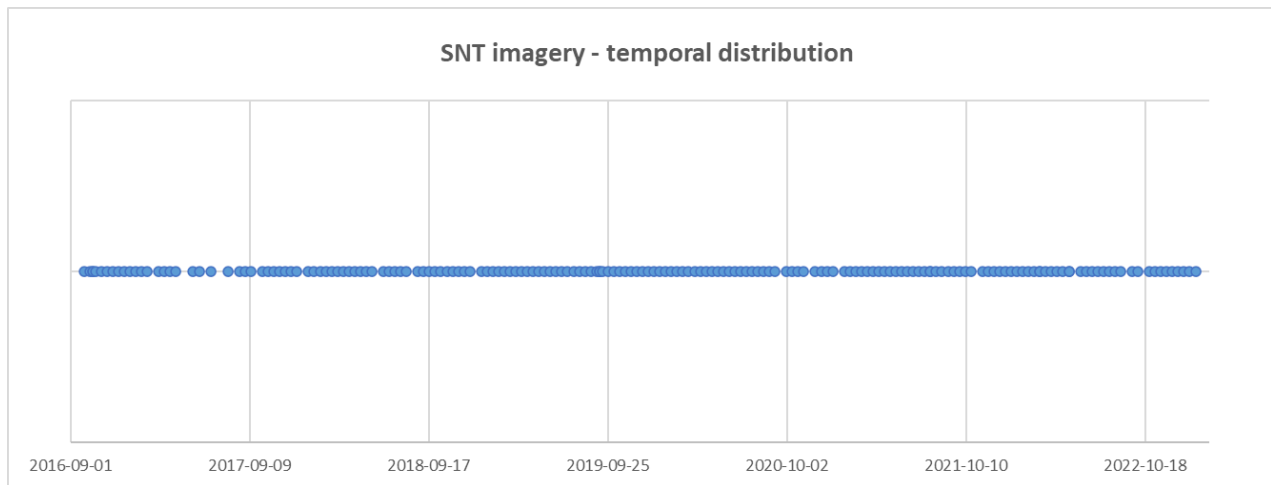
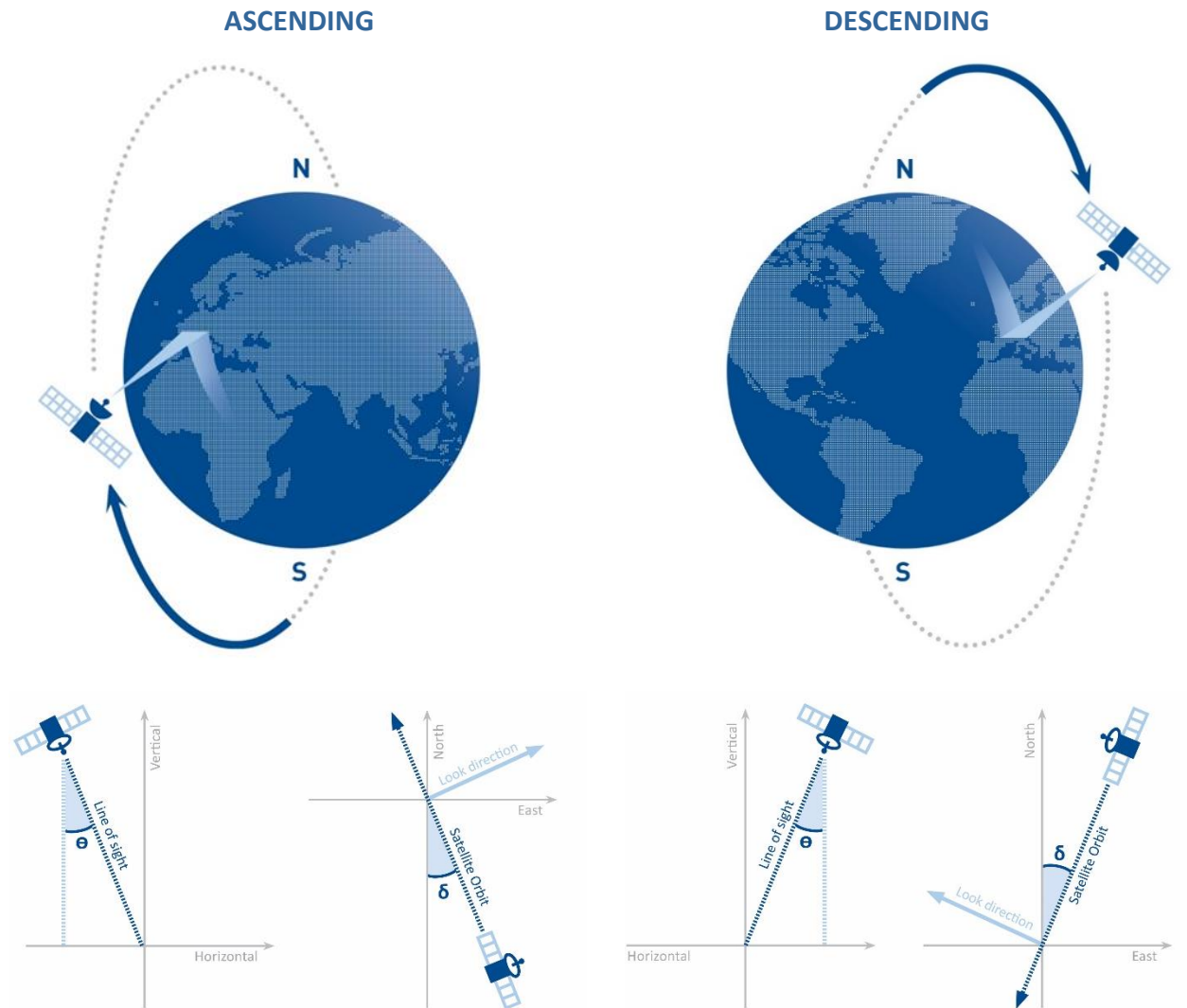


Figure 2: Temporal distribution of the SNT imagery processed for the current study.



©TRE Altamira

Figure 3: SAR satellites image the ground from ascending and descending orbits, according to the flight direction, from south to north (imaging to the east) and from north to south (imaging to the west), respectively. The satellite Line of Sight (LOS) is inclined with respect to the vertical and north-south direction (θ and δ angle, respectively). The current study used SNT historical imagery acquired over the AOI in ascending orbit.

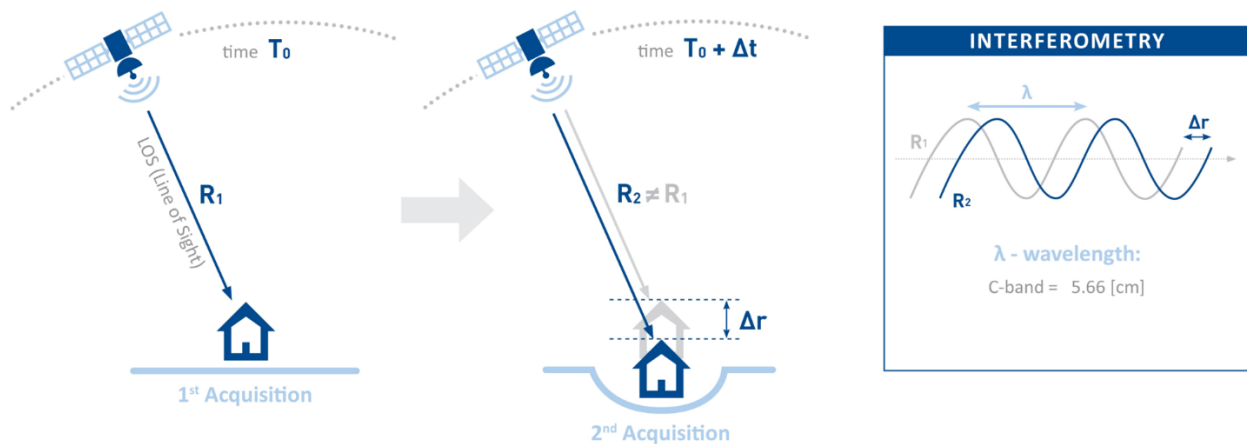
3. InSAR technology

This section provides an overview of InSAR technology and explains the characteristics of SqueeSAR measurements to introduce terminology and parameters used in describing the results of the current study. Further technical information on InSAR techniques can be found in the papers listed in the References.

3.1. SAR Interferometry – Basic principle

Interferometric Synthetic Aperture Radar (InSAR), also referred to as SAR Interferometry, is the measurement of signal phase change or interference over time (Rocca et al, 1997; Masonnet & Feigl, 1998; Burgmann et al, 2000; Ferretti et al., 2007).

When a point on the ground moves, the distance between the sensor and the ground target changes, which affects the phase value recorded by the SAR sensor. Figure 4 shows the relationship between ground movement and the corresponding shift in signal phase between two SAR signals acquired over the same area.



©TRE Altamira

Figure 4: Schematic showing the relationship between ground displacement and signal phase shift.

Any displacement of a radar target along the satellite LOS creates a shift in the phase of the radar signal that can be detected by comparing the phase values of two SAR images acquired at different times. The process referred to as SAR Interferometry (InSAR) is a comparison of two SAR images to identify and quantify that difference in signal phase.

An interferogram is a graphical representation of the differences in the phase values between two SAR acquisitions and corresponds to a matrix of numerical values ranging from $-\pi$ to $+\pi$. Interferometric fringes are generated when displacement causes the phase values to periodically repeat (from $-\pi$ to $+\pi$) over short distances. The process of converting the phase difference into displacement values is called “phase

unwrapping". Theoretically, wherever fringes occur, it is possible to measure displacement by calculating the number of fringes and multiplying them by half of the wavelength. However, in practice, interferometric phase values are a sum of different contributions (Figure 5), including displacement, atmospheric noise and decorrelation noise (i.e., changes in the physical and geometric properties of the ground targets, referred to as scatterers, between the acquisition time of two SAR images).

There are four main factors contributing to the interferometric phase ($\Delta\phi$):

- Displacement of the radar target (Δr) along the satellite Line of Sight (LOS),
- Topography (*topo*) arising from different viewing angles of the two satellite passes,
- Atmospheric component (α) arising from the wavelength distortion that occurs when signals enter and leave a moisture-bearing layer, and
- Noise (*noise*) due to phase decorrelation effects.

More precisely: $\Delta\phi = \frac{4\pi}{\lambda} \Delta r + topo + \alpha + noise$, where λ is the satellite wavelength.

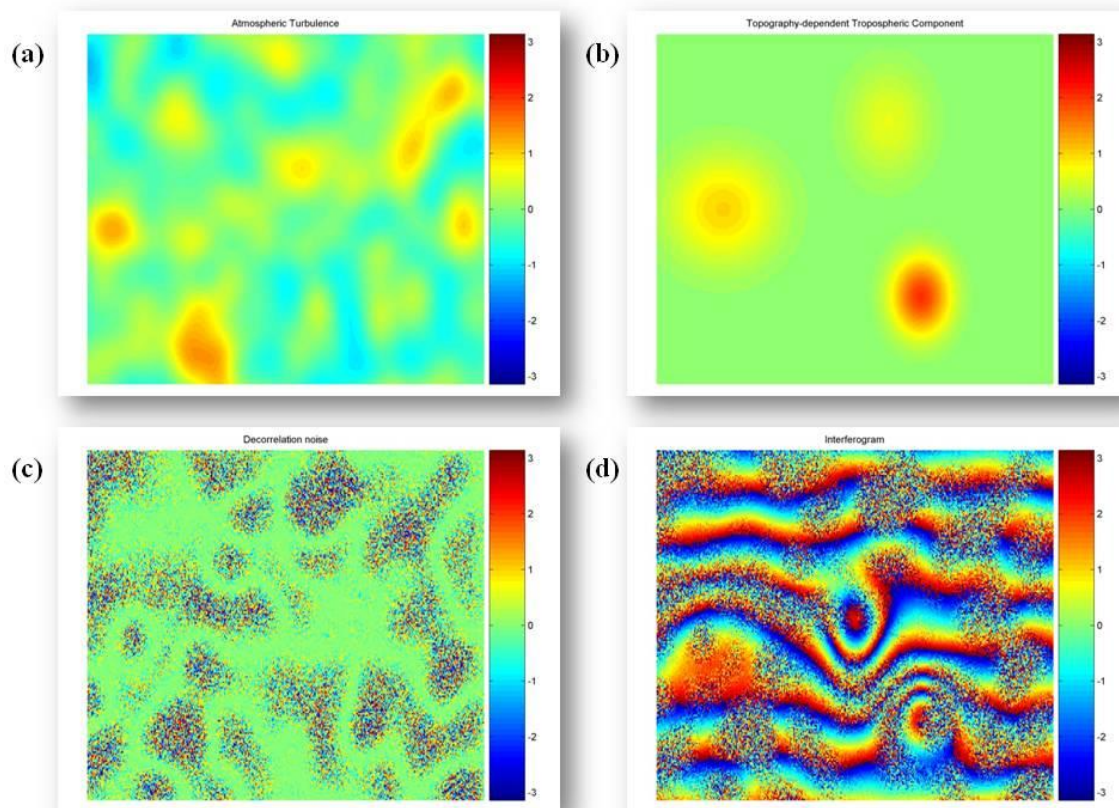


Figure 5: From Ferretti A. (2014): (a) Example of atmospheric turbulence effects on a SAR interferogram. The horizontal and the vertical axes correspond to the azimuth and range coordinates, respectively. (b) Example of topography-related atmospheric components. (c) Phase noise contribution affecting some areas within the imaged scene. (d) Example of resulting interferogram.

Topographic effects can be compensated by using a Digital Elevation Model (DEM) of the area of interest (Differential SAR Interferometry – DInSAR). The topography is converted to phase values to create a synthetic interferogram representing the topographic component, and is subtracted from the original interferogram to create a “differential interferogram” (DInSAR). If the DEM is accurate, any difficulties related to the estimation of surface displacement signals from a single SAR interferogram are then usually due to the presence of ground decorrelation effects and to the presence of atmospheric phase components superimposed on the signal of interest. In summary, limitations of conventional DInSAR analyses are due to (Ferretti A., 2014):

- Inaccuracies of the input DEM,
- Atmospheric effects, related to both topography (i.e., changes in elevation) and due to turbulence phenomena, and
- Phase decorrelation (i.e., absence of phase coherence between the two images) due to changes in the orbital trajectories from one acquisition to another, or variations in the nature and locations of elementary scatterers within the resolution cell.

Multi-interferogram advanced techniques were developed to identify coherent scatterers, estimate and remove atmospheric effects and calculate accurate time series of displacement, such as the PSInSAR™ technique (Ferretti et al., 2001) and the more recent SqueeSAR technique (Ferretti et al., 2011). The main objective of these techniques is the analysis of multi-image SAR data sets to estimate and remove residual DEM inaccuracies and atmospheric noise, using statistically based algorithms.

3.2. SqueeSAR

SqueeSAR is the advanced multi-image InSAR algorithm patented by TREA, which represents the third generation of InSAR technologies, after DInSAR and PSInSAR, and is the evolution of the latter. By analyzing a stack of SAR images acquired over a site, the SqueeSAR algorithm identifies and measures the movement of radar reflectors on the ground surface that remain visible and coherent throughout the period of the analysis (i.e., maintain high reflectivity and phase stability in all images being processed). Thanks to the statistical analysis of a dataset of images, the SqueeSAR technique estimates and removes the atmospheric noise component affecting the more basic DInSAR approach and provides high resolution and millimeter precision measurements of ground displacement in the form of a point cloud.

The density and distribution of measurement points (MP) identified by the analysis depends on the resolution of the imagery, the surface characteristics and its changes over time, and the topography of the area. In general, MP density and coverage increases with satellite resolution and decreases over:

- Low reflectivity areas (i.e., areas where the strength of the signal backscattered to the satellite is low, such as water or smooth surfaces),
- Areas where the satellite has visibility limitations, because of the Line of Sight (LOS) orientation with respect to the local topography, and
- Areas affected by decorrelation (i.e., the radar phase signal is not coherent over time), which in turn is generally associated with:
 - Variations of the surface characteristics (e.g., construction work, the disappearance of the radar reflector, etc.),
 - Presence of vegetation and/or water, and
 - Rapid movement, where decorrelation typically occurs for displacements greater than 1/4 of the satellite wavelength between two consecutive acquisitions.

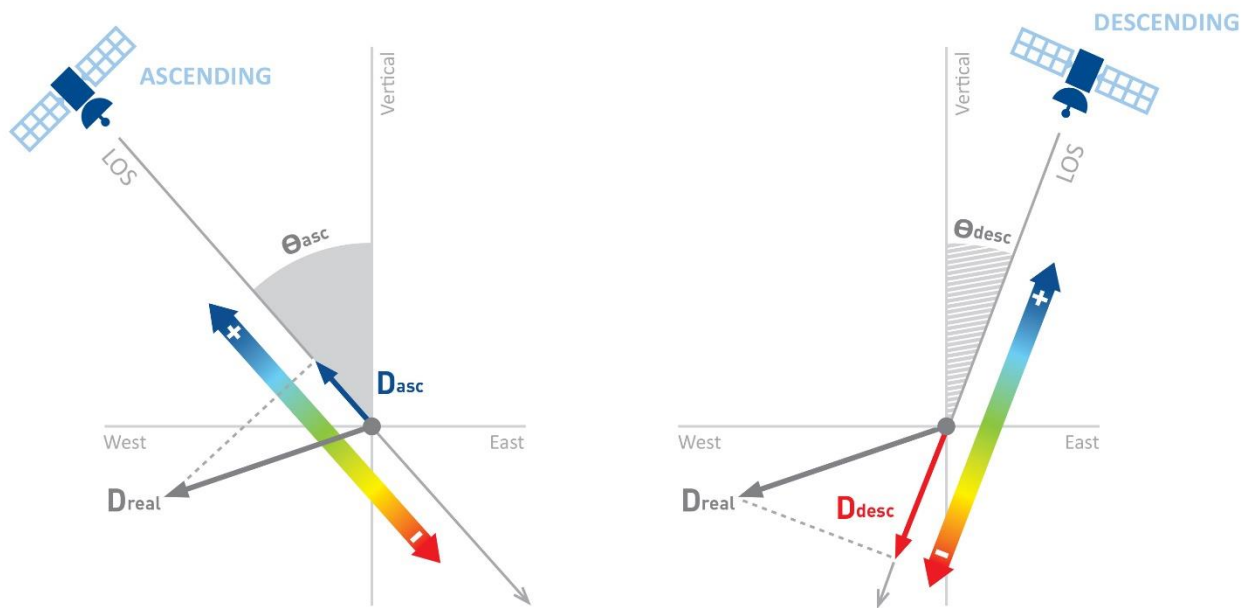
SqueeSAR measurements are differential in space and time: spatially they are related to a local reference point (REF) and temporally to the date of the first available satellite image. The REF is selected for its radar properties to optimize the quality of the measurements and is assumed to be motionless. The REF corresponds to the radar target with the highest coherence signal in all the images of the archive and that is not affected by displacement rate variations (non-linear movement or cyclical displacements) in the analysis period. If available, the absolute stability of the REF point can be validated using an independent Global Navigation Satellite System (GNSS) network. The selection of the REF is statistically based and imagery dependent. If the imagery changes (number of images and/or time span), the measurement point (MP) selected as the REF can change.

For each MP, SqueeSAR includes the following information:

- Position and elevation estimated with respect to the input DEM,
- Displacement time series (TS) representing the evolution of the displacement [mm] for each acquisition date compared to the first satellite image and measured along the LOS direction, and
- Annual average displacement rate [mm/yr], calculated as a linear regression of the displacement time series over the analysis period and referred to the REF.

3.2.1. 1-D LOS measurements

As SqueeSAR measurements are one-dimensional (i.e., away from or toward the satellite), the sign and value of the displacement depends on the orientation of the real displacement with respect to the LOS (Figure 6). By convention, negative values (from green to red) indicate movement away from the satellite, while positive values (from green to blue) indicate movement towards the satellite. Note that the same displacement produces different readings when viewed from different orbits and/or LOS angles.



©TRE Altamira

Figure 6: SqueeSAR measures the projection of real movement (D_{real}) onto the LOS. The same real movement (D_{real}) produces a different value from a different LOS (different inclination or different orbits). Positive values are indicated with colors from blue to green and denote movement towards the satellite; negative values and colors from green to red indicate movement away from the satellite. LOS measurements equal to zero may indicate stability or a real movement perfectly perpendicular to the LOS direction.

A LOS displacement (D_{LOS}) can be expressed as the sum of three factors:

$$D_{LOS} = D_{VERT} * H_{LOS} + D_{EW} * E_{LOS} + D_{NS} * N_{LOS}$$

where H_{LOS} , E_{LOS} and N_{LOS} are the LOS direction cosines (or versors) along the three directions (Vertical, North-South and East-West) and D_{VERT} , D_{EW} and D_{NS} are the three components of the real movement vector. The percentage of each component, D_{VERT} , D_{EW} and D_{NS} measured from the LOS direction depends on the specific orbit parameters and versors. However, due to the SAR satellite acquisition geometry (LOS generally inclined less than 45° with respect to the vertical direction and orbits less than 10° with respect to the north-south direction), InSAR has a higher sensitivity to vertical motion components, a marginally lower sensitivity to east-west motion component and a very low sensitivity to the north-south component.

It is noted that interpreting LOS displacement as vertical displacement (i.e., $D_{LOS} = D_{VERT}$) requires the assumption of negligible horizontal components ($D_{EW} = 0$ and $D_{NS} = 0$) of the real displacement vector. The error introduced by an unverified negligible horizontal component assumption is proportional to the amount of the horizontal component and increases with the LOS (θ) angle.

When both LOS ascending and descending measurements are available over the same area and overlapping period, it is possible to estimate the D_{VERT} and D_{EW} motion components by a trigonometric combination of LOS

readings on a regular grid of points. Although two-dimensional (2-D) measurements are generally easier to interpret than LOS data, they have a lower spatial resolution and do not correspond to single reflectors on the ground, but instead to the cell of a grid. For detailed analyses of localized movements and urban environments it is preferred to use full resolution LOS data.

3.2.2. Measurement precision and sources of inaccuracy

Since InSAR measurements are relative to a local reference point (REF), we refer to precision instead of absolute accuracy of the measurements. The estimation of both the MP displacement and MP location is part of the InSAR analysis, and we can distinguish between:

- Precision of the estimated displacement, and
- Precision of the location of a measurement point.

In general, the precision of multi-image InSAR displacement measurements is on the order of a few millimeters, while the precision with which the location of an InSAR MP is known is on the order of a few meters.

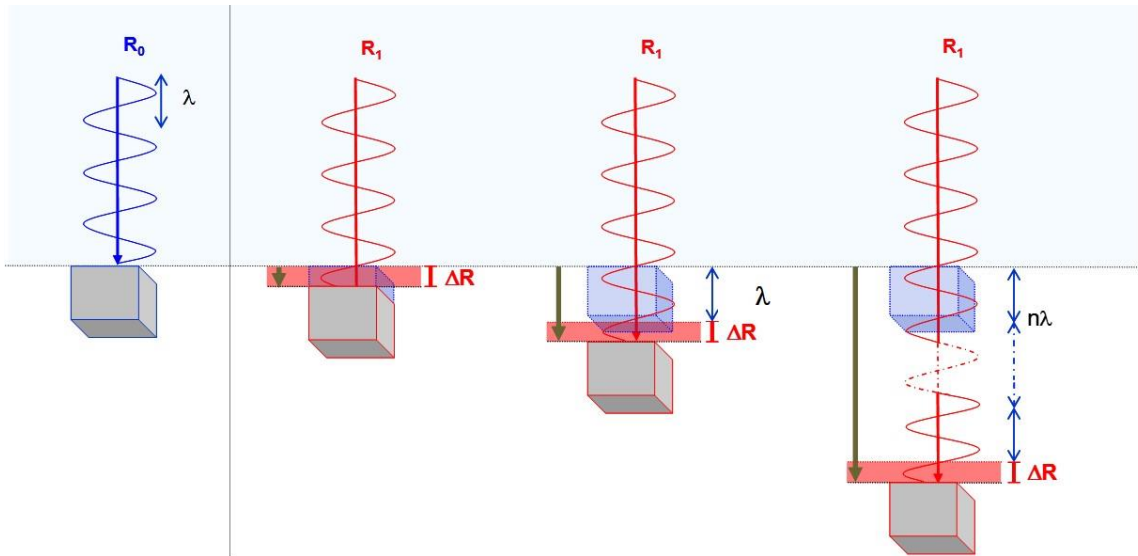
3.2.2.1. Displacement measurements

The main factors influencing the precision of InSAR displacement measurements are the coherence of the radar targets (i.e., phase stability over time), the power of the atmospheric noise and the quality of the analysis itself (i.e., the probability of phase unwrapping errors or unmodelled phase components).

Since the analysis is statistically based, these factors not only depend on the quality of each image, but also on the quality of the entire processed data set. In addition, the higher the spatial density of the InSAR point cloud and the quality of the data set, the lower the probability of phase unwrapping errors.

In a case of rapid displacement affecting single isolated targets, the phase unwrapping can be affected by an ambiguity of the phase (also known as “phase aliasing”). Figure 7 illustrates a case of phase aliasing. The grey solid represents a radar target. The target is represented at an initial R_0 distance (in blue), while in red there are three possible shifts to R_0 . Without prior information, the system is not able to estimate the correct number of wavelengths ($n\lambda$) that occurred, meaning that all three cases will indicate an equivalent ΔR shift measurement. Furthermore, it is necessary to consider both the displacement and the direction of motion. Theoretically, only displacement below $1/4$ of a wavelength will be correctly detected on single, isolated radar targets. Any greater displacement may be misinterpreted. In extreme cases, if the target moved exactly half a wavelength between two acquisitions the target would appear to be perfectly stable.

Note that these theoretical limits refer to rapid movements affecting single isolated radar targets. The ambiguities can be resolved in cases where the movement is spatially correlated and the MP density is sufficient for additional MPs to fall within the area of movement.

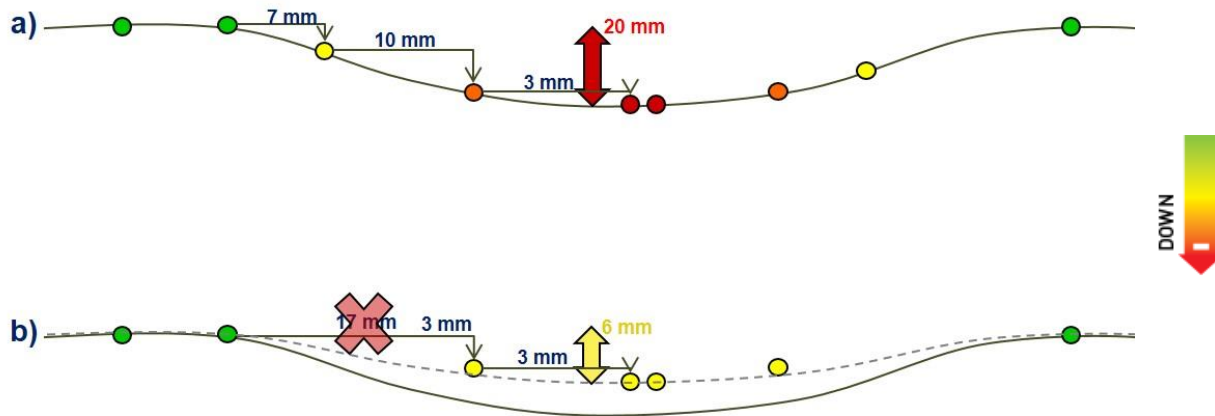


©TRE Altamira

Figure 7: Schematic of a sinusoidal phase of the electromagnetic wave incident on a moving target (grey solid). Without prior information, it is not possible to estimate the correct number of wavelengths ($n\lambda$) that occur and in all three cases illustrated above an equivalent ΔR shift is measured.

Figure 8 shows a schematic of a spatially correlated subsidence phenomenon. When the radar target density is sufficient, a correct phase unwrapping can be conducted and a total displacement higher than the $\lambda/4$ limit can be measured. In a case where the radar target distribution is not adequate, an incorrect phase unwrapping can cause an underestimation of the displacement.

The temporal distribution of the acquisitions also impacts the phase unwrapping correctness: the higher the acquisition frequency, the greater the ability to correctly unwrap and describe rapid movements.



©TRE Altamira

Figure 8: Schematic of spatially correlated subsidence. The measurement points are color-coded according to the downward displacement measured along the surface profile. Considering a C-band satellite, a total displacement of 20 mm (higher than the $\lambda/4$ limit of 14 mm) can be measured when the MP are well distributed along the subsiding profile (a). When the measurement point distribution is not adequate, an underestimation of the real displacement (i.e., 6 mm instead of 20 mm) occurs (b).

In summary (refer to Ferretti et al. 2014 for a detailed description of all sources of inaccuracies), the precision of SqueeSAR measurements:

- Increases with the number of processed images, the length of the period of the analysis, the frequency of acquisitions and the coherence of the signal, and
- Decreases with the presence of gaps in the acquisitions, strong atmospheric disturbances, variations of the surface reflectivity and decorrelation in the period of the analysis.

In particular, SqueeSAR measurements are provided with three precision indices:

- The coherence of the phase signal over time (COHERENCE), which is imagery-dependent and normalized to a value between 0 and 1. The higher the coherence, the higher the precision of the measurements. Typically, points with a coherence <0.5 should be considered with caution in the analysis of the results because of their lower radar signal stability.
- The displacement rate standard deviation (V_STDEV), which provides an indication of the precision of the annual displacement rate (1 sigma) with respect to the REF. The displacement rate standard deviation increases with the distance of the point from the REF. Typical V_STDEV values obtained with an InSAR analysis of a dataset of at least 30 images for a point located less than 1km from the REF are on the order $\pm 1\text{mm/yr}$.
- The average time series error bar (STD_DEF), which provides an indication of the precision of single displacement measurements of the time series. This parameter is calculated as the standard deviation of the residuals with respect to an analytical model (i.e., how well the model fits the displacement time series). The model is selected individually for each MP with an advanced Model

Order Selection technique (from Cherkassky et al., 1996), that takes into account the quality of the imagery (number of images, time span and possible gaps in the acquisitions). Typical STD_DEF values obtained with an InSAR analysis of a dataset of at least 30 images are on the order of ± 5 mm. It is noted that the STD_DEF value is statistically calculated for each measurement point and consists of the average error bar (1 sigma) of the whole time series of displacement. Single measurements within the time series may have a lower or higher quality based on the specific satellite acquisition characteristics, such as the atmospheric noise present at the time of the acquisition, the accuracy of the orbital path and decorrelation noise.

When analyzing the measurements and precision values, it should also be noted that, assuming the error has a Gaussian distribution, a ± 1 sigma error bar gives confidence intervals around the mean error for 68.2% of the measurements, a ± 2 sigma error bar for 95.4% of the measurements and a ± 3 sigma error for 99.6% of the measurements.

3.2.2.2. MP location

The geographic coordinates and elevation of a measurement point depend on its SAR coordinates and are estimated with the InSAR analysis. The higher the spatial resolution of the satellite sensor and the input DEM, the higher the precision of the geocoding. However, since the elevation of a measurement point is estimated from the phase values of the InSAR dataset, the geolocation error also depends on the quality of the analysis and increases with the quality of the imagery (i.e., the number of images, frequency and temporal coverage of the acquisitions), the coherence of the signal and the density of points.

Table 4 reports the typical precision values associated with the coordinates of MP at mid-latitudes using different SAR imagery and Figure 9 shows the typical location precision values obtainable with the low-resolution SNT imagery used for the current study, which is ± 8 m in the NS direction, ± 12 m in the EW direction and ± 8 m in the vertical direction.

For the current analysis, the measurement point location and elevation have been estimated with respect to the WGS84 reference ellipsoid, using the Shuttle Radar Topography Mission (SRTM) DEM (<https://www2.jpl.nasa.gov/srtm/>) as input. The data was further orthorectified using a 2018 Digital Terrain Model (DTM) of the Site-specific AOI available on the USGS GIS download portal (<https://www.usgs.gov/the-national-map-data-delivery/gis-data-download>), reporting a +23.5 m shift between the WGS84 ellipsoid and the Site-specific DTM.

Since all InSAR measurements are relative to the reference point (REF), the absolute accuracy of the MP locations also depends on the location accuracy of the selected REF. The absolute location of the REF with respect to the International Terrestrial Reference System (ITRS) is best verified using an independent GNSS

(Global Navigation Satellite System). For this study, there were no reliable GNSS stations near the REF but in most applications the relative accuracy of the point coordinates (i.e., measurement of how well the vector between two points is measured) is much more important than absolute accuracy, since any systematic shift affecting a large area can be dealt with quite easily and, in any case, these shifts do not typically compromise data interpretation.

Satellite	Band	Wavelength [cm]	Pixel resolution RGxAZ [mxm]	North-South [m]	East-West [m]	Elevation [m]
SNT	C-band	5.9	20x5	± 8	± 12	± 8
Cosmo-SkyMed	X-band	3.12	3x3	± 1	± 1	± 0.5
TerraSAR-X (<i>Stripmap</i>)	X-band	3.11	3x3	± 1	± 3	± 1.5

Table 4: Characteristics of the main SAR satellites and typical precision values (1 sigma) associated to the UTM coordinates of a MP at mid-latitudes. Values are with respect to a MP less than 1 km from REF and a dataset of at least 30 SAR images.

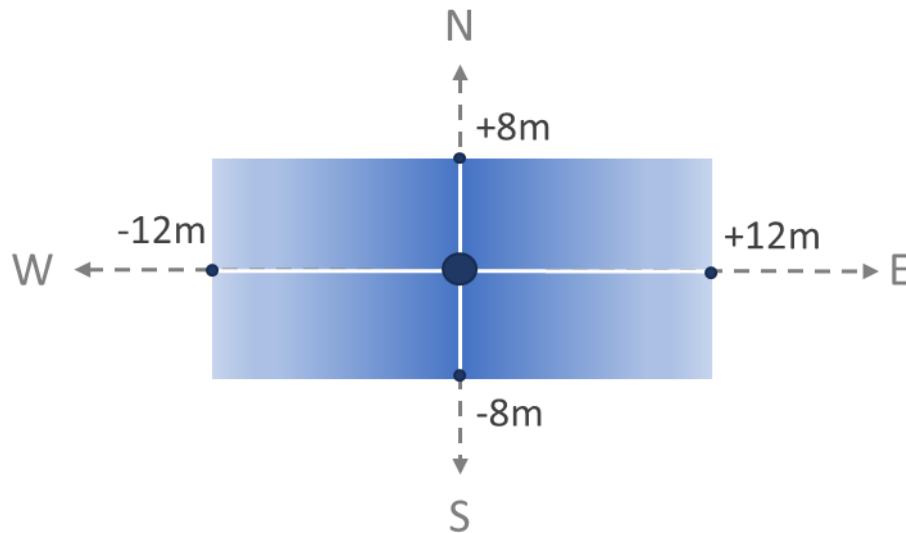


Figure 9: Typical precision of the point location associated with a SNT analysis. Values are with respect to a MP less than 1 km from REF and a data set of at least 30 SAR images.

4. Results

This section provides an overview of the results obtained over the area of interest. Annual displacement rate, acceleration and average seasonal maps are presented with the intent of highlighting possible areas of displacement and/or non-linear trends as input for the Data Analysis (Section 5). Refer to Section 3.2.2.1 for details on the quality parameters.

4.1. Overview

The SqueeSAR processing of the SNT imagery produced full resolution measurements in the form of point clouds. Each measurement point (MP) comprises a time series of 1-D LOS displacement (i.e., cumulative displacement with respect to the first radar image of the data stack, measured along the satellite Line of Sight). Three quality parameters are provided for each MP:

- Coherence of the phase signal (COHERENCE), which is a value normalized to 0-1 that provides an indication of the quality of the interferometric coherence (i.e., stability of the phase signal over time),
- Displacement rate standard deviation (V_STDEV), which provides an indication of the precision of the annual displacement rate with respect to the reference point (REF) [mm/yr], and
- Average time series error bar (STD_DEF), which provides an indication of the precision of single displacement measurements of the time series [mm].

Each MP has a specific time series and trend, but the following parameters are calculated from the time series of displacement to support and facilitate the data analysis and identification of non-linear trends:

- Annual displacement rate [mm/yr], which provides an indication of the rate of motion and is calculated as linear regression of the time series of displacement (i.e., by fitting a first order polynomial model $[(dt) = a + bt]$ to the time series of displacement),
- Acceleration over the period of the analysis [mm/yr²], which provides an indication of possible accelerating or decelerating trends and is calculated by fitting a second order polynomial model $[(dt) = a + bt + ct^2]$ to the time series of displacement, and
- Average seasonality [mm], which provides an indication of possible cyclic deformation trends and is calculated by fitting a polynomial model with a seasonal component $[(dt) = a + bt + ct^2 + A \cos(\frac{2\pi T}{365} + \varphi)]$ to the time series of displacement.

Table 5 provides a summary of the results, including the reference point location, average point density and quality of the measurements. Overview maps are reported in Figure 10 to Figure 12, where the measurement points are color-coded according to the annual LOS displacement rate (mm/yr), the average amplitude of seasonality (mm) and acceleration (mm/yr²) in the period of the analysis, respectively.

The REF is selected for its radar properties to optimize the quality of the measurements and is assumed to be motionless. The stability of the REF point was evaluated through careful examination of historical aerial imagery and the measurements were compared to absolute ground displacement measured at available GPS stations within the Local AOI. GPS time series of ground displacement were used to “ground truth” the InSAR, providing time and location specific representations of ground movement that is directly relatable to the observed time series of relative displacement measured from InSAR. These analyses are further discussed under Section 5 of this report.

Table 5: Summary of the SqueeSAR results

Analysis characteristics	SNT SqueeSAR results
Period covered (YYYY-MM-DD)	2016-09-27 to 2023-01-30
Number of images processed	177
Reference point location*	X=273,084.986, Y=174,338.227
Number of MP	7,393,970
Average displacement rate standard deviation (V_STDEV)	< ±1mm/yr
Average time series error bar (STD_DEF)	±3.5 mm
Minimum coherence (COHERENCE)	0.52

* Provided in NAD1983_HARN_StatePlane_Florida_East_FIPS_0901 (EPSG: 2777) coordinates

Table 5 reports the average displacement rate standard deviation and error bars obtained with the analysis. However, while the table indicates the average values of all measurement points within the dataset, each measurement point also has a specific set of quality parameters. It is also noted that single points within the time series may be less accurate than indicated by the average time series error bar (STD_DEF) due to the presence of noisy images. Atmospheric conditions or surface changes may cause a temporary loss of coherence resulting in noisy intervals within the time series. Sources of possible inaccuracies are further discussed in section 5.2. However, it is generally observed that construction work and surface changes may cause temporary decorrelation noise within the time series and reduce point coverage in the case of persistent surface changes (i.e., loss of measurement points because of changes to the ground surface). Consequently:

- Gaps or low point density are observed over areas affected by prolonged construction or that are vegetated/sandy, where surface changes are caused by the nature of the ground.
- Trend changes observed in the time series during construction activities should be interpreted with caution even if the overall quality parameters of the points are acceptable.

The overview maps do not highlight the presence of regional trends. However, localized areas of movement are observed and are discussed in Section 5.3, together with transects of specific interest defined by NIST.

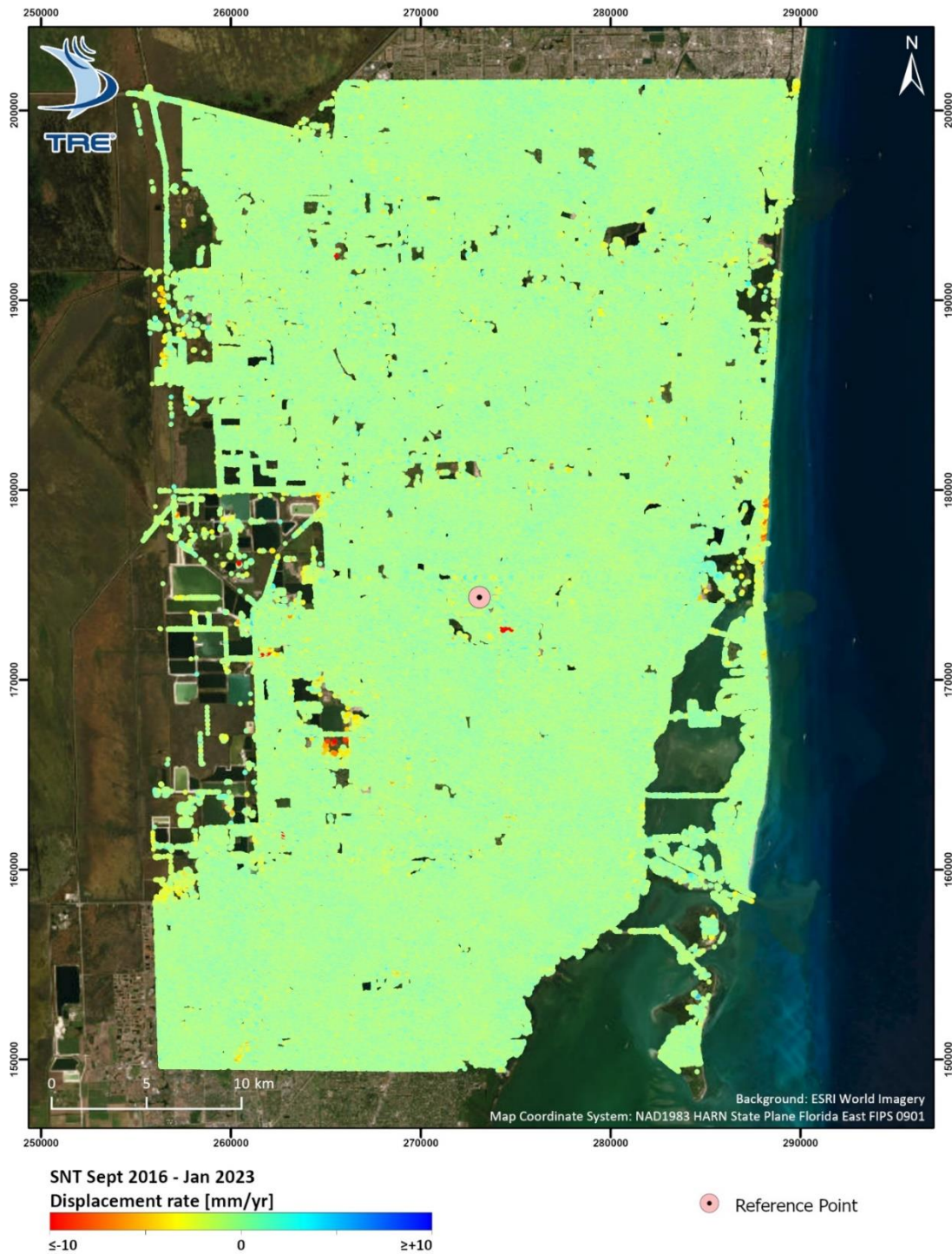


Figure 10: SNT results, visualized by annual displacement rate (mm/yr).

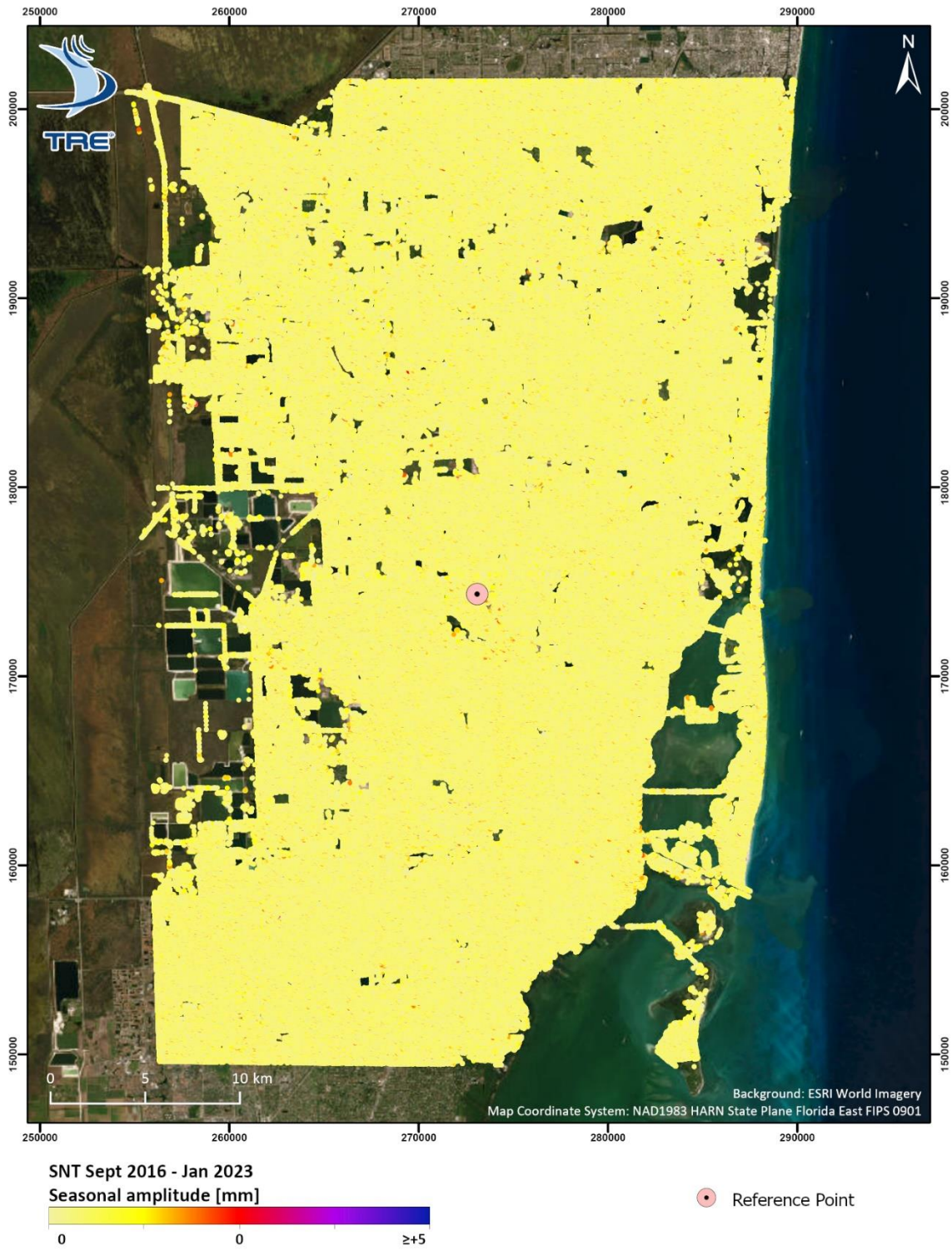


Figure 11: SNT results, visualized by average amplitude of seasonality (mm).

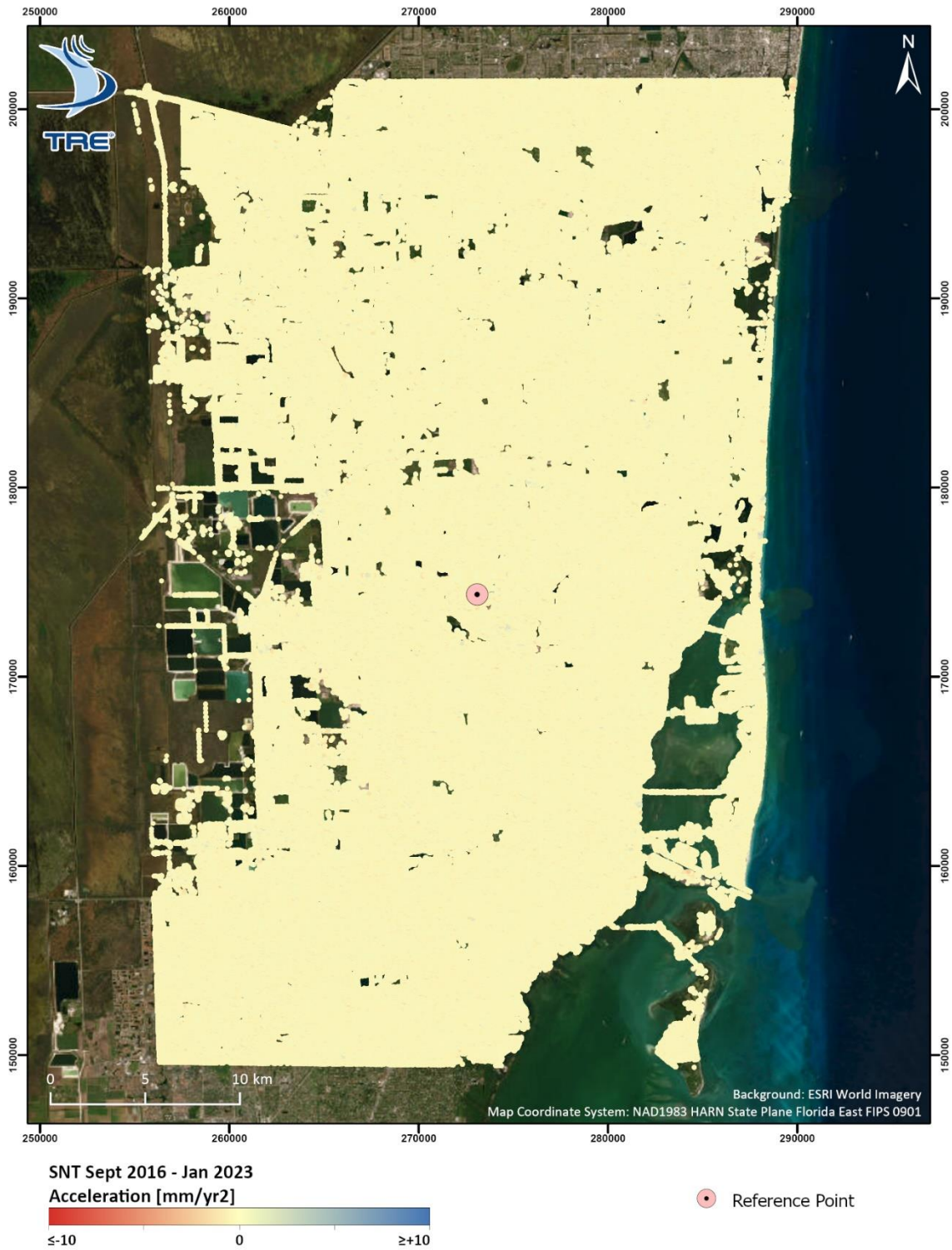


Figure 12: SNT results, visualized by acceleration in the period of the analysis (mm/yr²).

5. Data Analysis

An analysis and interpretation of the InSAR data was performed by Exponent, Inc. (EX) to characterize and quantify observed ground displacement trends within the AOI and in the context of environmental processes such as geology, hydrology and anthropogenic activity. This effort was aimed at an interpretation, analysis and documentation of observed spatial and temporal trends throughout the AOI and with specific attention to the transects of interest agreed upon with NIST.

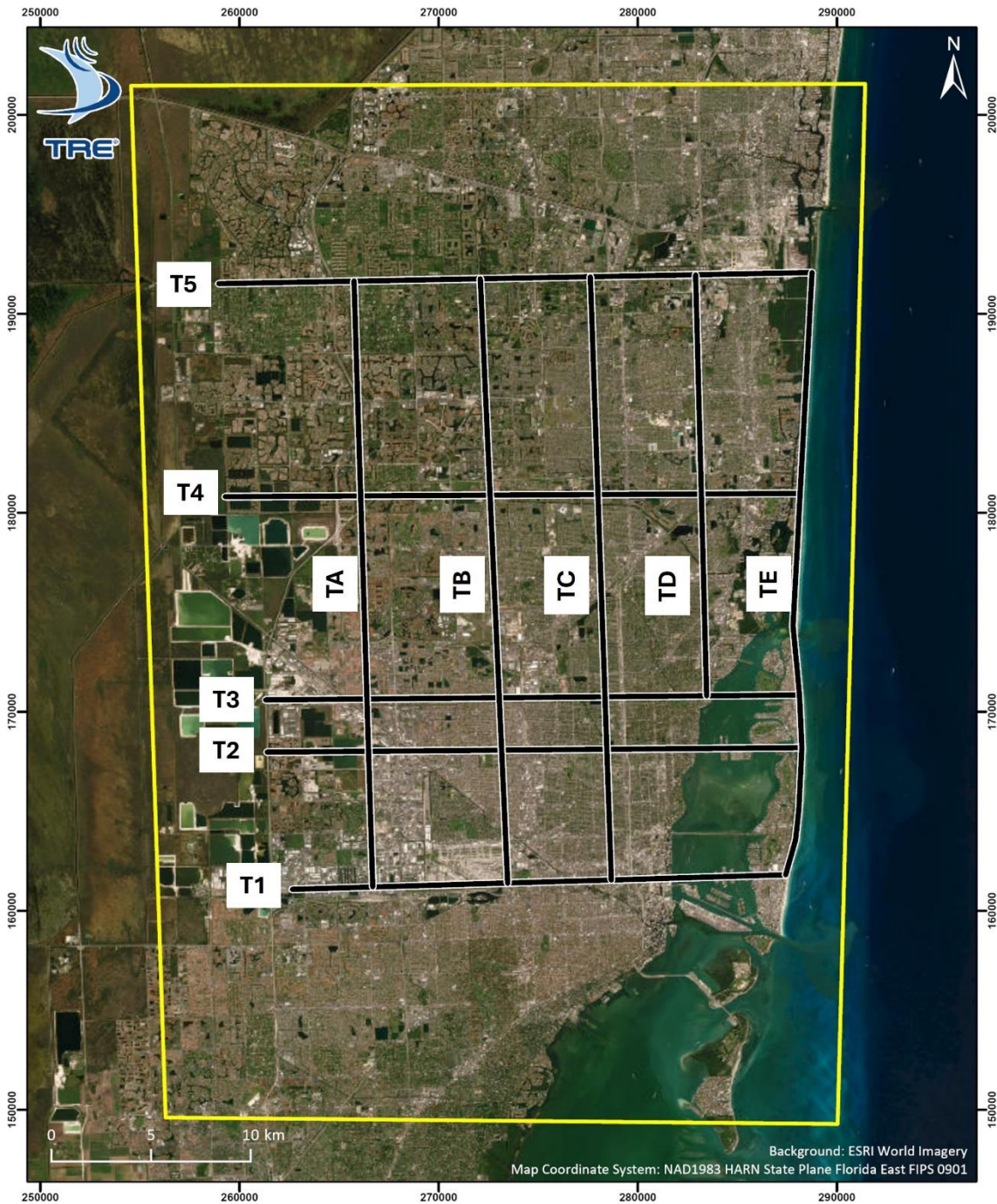
NIST identified 10 transects across the AOI in the North-South and East-West directions (Figure 13). The transects were intended as cross-sectional representations of the displacement rates for InSAR MPs located along each transect. To accommodate for uncertainty in the location accuracy of the MPs, each transect was buffered by ± 10 m and MPs were projected orthogonally onto the transects. All transects are included in Appendix 1 and the most significant ones are also included and discussed in this section.

The evaluation and analysis of observed spatial and temporal trends was performed in the context of the InSAR data, available subsurface geological and hydrological data, and historical tidal data. Potential sources of error and uncertainty, including their effects on the resulting data, were also identified, analyzed and documented.

This section presents the data considered, the analysis methodology and subsequent interpretive findings of the analysis. The analysis aims to address the following:

- Summary of data sources incorporated in the analysis (Section 5.1)
- Evaluation of the InSAR data and sources of potential errors (Section 5.2)
- Analysis of displacement trends over the AOI (Section 5.3)

Objective relevant observations and conclusions related to the regional displacements over time are summarized in Section 6.



 Area of Interest (AOI)

Figure 13: Location of the 10 transects defined by NIST.

5.1. Summary of Ancillary Data

Ancillary data was gathered to assess specific environmental effects such as geologic conditions, tidal effects, groundwater conditions and anthropogenic effects across the AOI. The data was primarily collected from publicly available sources and supplemented by data made available through NIST.

5.1.1. Historical GNSS Data

Historical data was considered from a total of 8 permanent GPS stations located within the Local AOI (Figure 14). The purpose of using this data is to validate the stability of the selected local reference points (REFs) and the accuracy of the InSAR time series by ground-truthing measured displacement trends. No permanent GPS stations or long-term campaign GPS data were available within the Site-specific AOI. The station locations are shown in Figure 14 and a list of the GPS station data is included in Table 6. The stations were selected based on their temporal coverage and quality of data. The data was acquired from the MAGNET GPS Network through the Nevada Geodetic Laboratory which automatically ingests and processes data from existing GPS stations nationwide¹ (Blewitt & Hammond, 2018).

Table 6: Permanent GPS stations considered in analysis. Coordinates are reported in WGS84 decimal degrees.

Station Name	Latitude	Longitude	Record Start (YYYY-MM-DD)	Record End (YYYY-MM-DD)
AOML	25.735°	-80.162°	1997-11-20	2004-04-04
FCHO	25.908°	-80.125°	2020-02-13	2023-02-11
FCI1	25.906°	-80.137°	2020-02-17	2023-02-11
FLD6	25.780°	-80.376°	2017-07-01	2023-02-11
FLMB	25.783°	-80.137°	2017-07-01	2023-02-11
FLN2	25.966°	-80.167°	2017-07-01	2023-02-11
N300	25.731°	-80.162°	2018-06-07	2023-02-11
ZMA1	25.825°	-80.319°	2003-04-11	2023-02-11

¹ <http://geodesy.unr.edu/magnet.php>

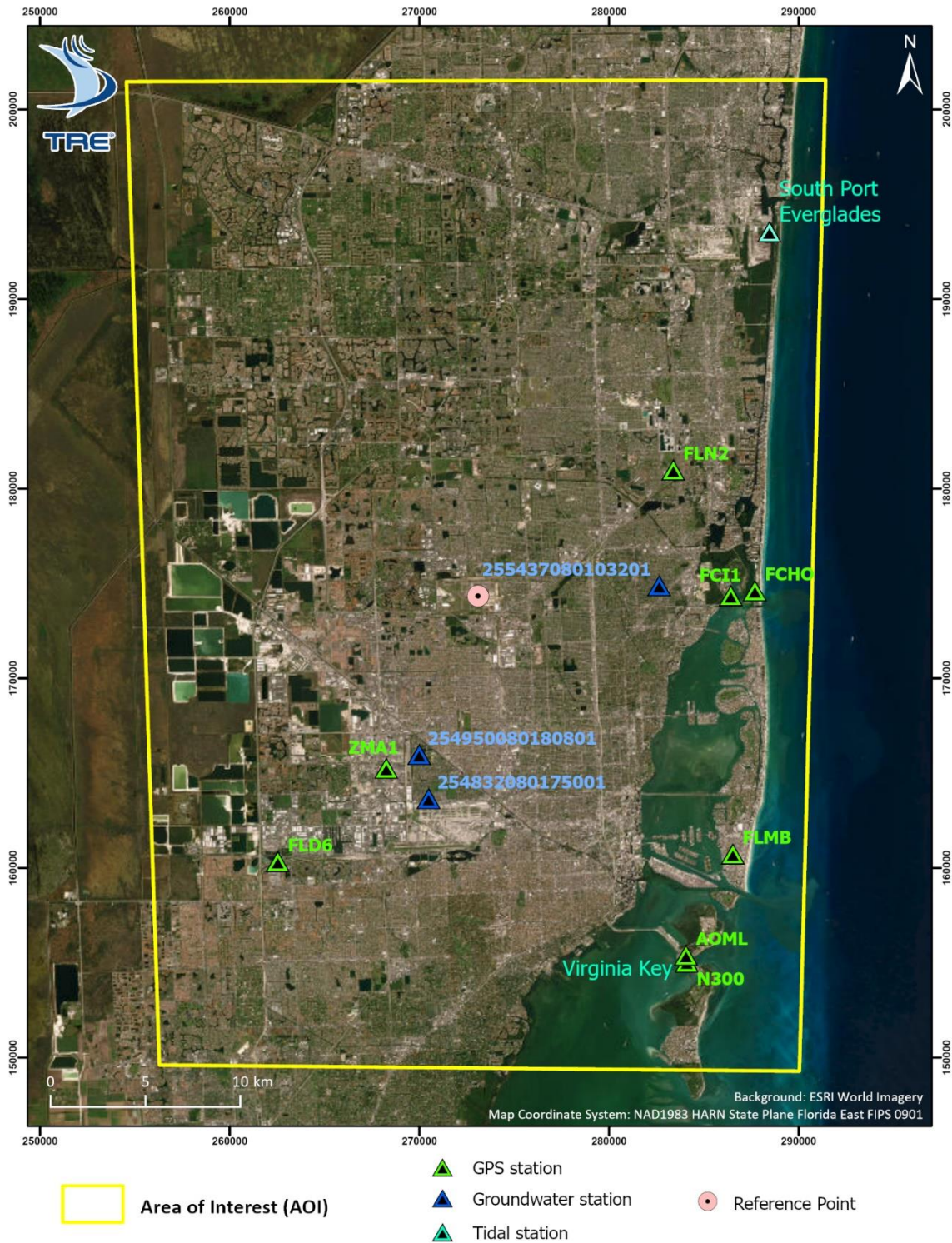


Figure 14: Location of GNSS, tidal and groundwater stations. The map also includes the location of the InSAR reference point.

5.1.2. Historical Tidal Data

Historical tidal data was collected for the two tidal stations within the AOI (Figure 14). The purpose of using this data is to evaluate whether the InSAR time series analyses are affected by seasonal tides, particularly along coastal areas. A list of the acquired tidal station data is included in Table 7. The data were acquired from the National Oceanic and Atmospheric Administration (NOAA) which maintains historical monitoring records for oceanic tides and currents nationwide².

Maximum tidal fluctuations during the period of interest ranged between 1.7 m and 2 m. The mean tidal range for these stations was between approximately 0.6 m to 0.76 m with a diurnal range of between 0.7 m and 0.85 m. Importantly, due to the temporal frequency of the InSAR data, diurnal temporal trends cannot be resolved, and only seasonal trends were considered.

Table 7: NOAA Tidal station data considered in analysis. Coordinates are reported in WGS84 decimal degrees.

Station Name	Station ID	Latitude	Longitude	Record Start (YYYY-MM-DD)	Record End (YYYY-MM-DD)	Measurement Frequency
Virginia Key, Biscayne Bay, FL	8723214	25.731361°	-80.161854°	2016-01-01	2023-04-30	Diurnal (Highest and Lowest)
South Port Everglades, FL	8722956	26.078777°	-80.115901°	2018-01-31	2023-04-30	Diurnal (Highest and Lowest)

5.1.3. Historical Groundwater Monitoring Data

Historical groundwater monitoring data were considered across the AOI (Figure 14). The purpose of using this data is to evaluate whether the InSAR time series analyses are affected by seasonal or anthropogenic variations in groundwater levels. Groundwater monitoring data was collected and analyzed for three wells near specific points of interest to the analysis of the SNT InSAR time series. A list of the acquired groundwater monitoring well data is included in Table 8. The data were acquired from the United States Geological Survey (USGS) which maintains historical monitoring records for groundwater wells nationwide³.

Over the period of observation, the groundwater level generally fluctuated approximately between 0.7 m and 1.6 m. Groundwater elevations near the coast exhibited seasonal fluctuations ranging between

² <https://tidesandcurrents.noaa.gov/>

³ <https://waterdata.usgs.gov/nwis/gw>



approximately 0.6 m and -0.9 m elevation (NAVD88) and between approximately 0 m and 1.5 m depth below the ground surface. Inland groundwater levels (approximately 20 km West of the coast) ranged between approximately -1.7 m and -0.1 m elevation (NAVD88) and between approximately 1 m to 2.6 m depth below the ground surface.

Table 8: USGS Groundwater monitoring well data considered in analysis. Coordinates are reported in WGS84 decimal degrees.

Station Name	Latitude	Longitude	Record Start (YYYY-MM-DD)	Record End (YYYY-MM-DD)	Monitoring Frequency
254950080180801	25.830833°	-80.301889°	2003-04-11	2023-02-11	daily
254832080175001	25.809944°	-80.297139°	2003-04-11	2023-02-11	daily
255437080103201	25.910722°	-80.175167°	2003-04-11	2023-02-11	daily

5.1.4. Historical Subsurface Geological Data

Geological data was acquired to characterize subsurface conditions across the study area and identify the potential for expression of surface processes related to geological formations. The data were primarily acquired from the USGS (https://ngmdb.usgs.gov/ngmdb/ngmdb_home.html,^{4,5,6,7,8,9}), which maintains regional geological records nationwide. Geological maps of the AOI illustrate that subsurface conditions across that area primarily consist of limestone formations, overlain by varying degrees of quaternary sand, organic silt and peat deposits, as well as anthropogenic fills. The surficial deposits range between approximately zero to 8 m in thickness, and the limestone formations can be encountered beginning at

⁴ Duncan J., 1993, Geologic Map of Dade County Florida, *Open-File Map Series 67*, Florida Geological Survey, Department of Natural Resources, Map.

⁵ *Geologic Well and Borehole Data Map*, Map Direct, Florida Geological Survey, Florida Department of Environmental Protection, <https://ca.dep.state.fl.us/mapdirect/?webmap=158cbdbaeb6245438e5e7be30368f7e8>

⁶ Matson, G.C., and Clapp, F.G., 1909, A preliminary report on the geology of Florida with special reference to the stratigraphy, Florida Geological Survey, *Annual Report no. 2*, p13-173

⁷ Matson, G.C., and Clapp, F.G., Sanford, S., 1909, *Geologic and Topographic Map of Florida*, Prepared by the United States Geological Survey, Map.

⁸ Scott, T.M., Campbell, K.M., Rupert, F.R., Arthur, J.D., Missimer, T.M., Lloyd, J.M., Yon, J.W., and Duncan, J.G., 2001, *Geologic Map of the State of Florida*, Florida Geological Survey & Florida Department of Environmental Protection, Map Series 146, scale 1:750,000. Revised 2006

⁹ Scott, Thomas M.P.G. #99, Text to Accompany the Geologic Map of Florida, *Open-file Report 80*, Florida Geological Survey, 2001.

depths of approximately zero to 8 m. The limestone formations consist primarily of limestone with interlayered and intermixed sand and cemented sand deposits.

Limestone formations may be subject to the development of dissolution caverns (i.e., karst formation) which can result in ground subsidence. The Florida Department of Environmental Protection maintains a record of historical ground subsidence incidents¹⁰. Throughout the entire AOI, only one instance of ground subsidence (3.1 m in width) was reported within the period of study but was too small to be detected by the SNT InSAR time series analysis which has a resolution of approximately 20 m. Data for this reported instance of ground subsidence is included in Table 9.

Table 9: Florida Department of Environmental Protection incident report data. Coordinates are reported in WGS84 decimal degrees.

Reference Number	Latitude	Longitude	Date Reported (YYYY-MM-DD)	Width (m)
87-002, 87-003	25.721738°	-80.37525°	2019-09-30	3.1

5.1.5. Historical Aerial Photos

Aerial photographs from publicly available sources and provided by NIST were reviewed. The purpose of reviewing these data was to incorporate known infrastructure development activity into the interpretation of the InSAR time series, to evaluate areas and periods of potential low coherence and decorrelation, as well as to identify potential areas of subsequent displacement. Within the AOI, infrastructure development activity was evaluated on the basis of observed trends in the SNT InSAR time series analysis data and in an effort to interpret them. Those observations are discussed in Section 5.3

5.2. Evaluation of the InSAR data and sources of errors

Evaluation and validation of the InSAR time series data involved three stages.

- First, the REF point location was evaluated, to verify that it was not affected by changes in the ground surface.
- Second, the InSAR time series were “ground truthed” against observed ground displacement trends measured at selected GPS stations.

¹⁰ <https://floridadep.gov/fgs/sinkholes>

- Finally, the InSAR time series were interpreted in the context of processes observed from the acquired ancillary data.

Ground displacement tracking by permanent GPS located within the AOI provides a time-specific representation of ground displacement that is directly relatable to the observed relative displacement trends measured from InSAR in the same area and at the same time. Three GPS stations (FCI1, FLMB and ZMA1) were selected on the basis of their geological setting, proximity to other ancillary data (e.g. groundwater monitoring wells), and the completeness of their data over the period of study. Stations FCI1 and FLMB were selected based on being the most complete GPS data sets available in close proximity to tidal and groundwater monitoring data. Station ZMA1 was selected based on being the most complete GPS time series available over the entire period of study, its proximity to groundwater monitoring data and for being located at a distance from the coast. Since the continuous GPS stations and the REF are located within the same tectonic environment and on a relatively flat topography, ground displacement trends measured in the InSAR data were assumed to be primarily attributed to vertical motion and only compared against the vertical component of the GPS time series. For this comparison, the vertical GPS components were projected to the specific SNT LOS direction using the orbital parameters, as described in Section 3.2.1.

5.2.1. Evaluation of the REF point

The evaluation of the REF point location was performed based on aerial imagery spanning the period of study, to assess whether the REF point locations were affected by visible alterations of the ground surface. Based on a careful review of aerial imagery, the REF point appears to be located on stable structures and no visible changes to the structures or to the surrounding ground surface were observed.

5.2.1.1. Data validation at GPS Station FCI1

GPS station FCI1 was selected for validation of the SNT InSAR time series because it is located in a coastal area affected by tidal fluctuations, it is near a groundwater monitoring well, it has relatively complete temporal coverage over the period of study, the area does not appear to have been altered by anthropogenic activity over the period of study, and the area has sufficient InSAR measurement points (Figure 15).

FCI1 was compared against data from groundwater monitoring well number 255437080103201 (approximately 4 km to the west) and data from the South Port Everglades, FL tidal gauge (approximately 20 km to the North). As illustrated in Figure 16, groundwater variability is directly correlated to tidal fluctuations on a semi-annual basis (with a correlation coefficient of approximately 0.7, considering 180-day moving averages). As illustrated in Figure 17, the FCI1 vertical time series data (adjusted to reflect the satellite LOS direction, as described in Section 3.2.1) are also closely correlated with the long period fluctuations in the groundwater and tidal data (with a correlation coefficient of approximately 0.6, considering 180-day moving

averages). As illustrated in Figure 18, the average SNT InSAR displacement time series for the selected data does not exhibit a clear seasonal trend beyond the error of the displacement time series. A correlation analysis between a 90-day moving average of the SNT InSAR data and the groundwater data (90 day moving average reflecting seasonal changes) suggests a correlation coefficient of approximately 0.1. This can indicate that the entire Local AOI is affected by seasonal fluctuations that cannot be detected with an InSAR analysis because the InSAR REF is also affected, or that the seasonal fluctuations are below the precision of the InSAR results.

The correlation between the tidal data and groundwater data confirms the expected relationship between these two components. The correlation between the GPS data and short period fluctuation in the groundwater data suggests that the seasonality observed in the GPS data is related to the short period of fluctuation in the groundwater data. While the InSAR data exhibits variability, that variability is well within the error of the displacement time series and does not capture the seasonal fluctuations visible in the groundwater and GPS time series, as discussed above.

The ground surface fluctuations captured by the InSAR time series produced, on average, approximately 2.5 mm (LOS) of movement for long period seasonal displacements (with an approximate 180-day cycle), compared to average tidal fluctuations of approximately 500 mm. The average ground surface fluctuations captured by the InSAR time series for short period seasonal displacements (with an approximately 90-day cycle) was approximately 5 mm (LOS), compared to average groundwater fluctuations of approximately 1000 mm.

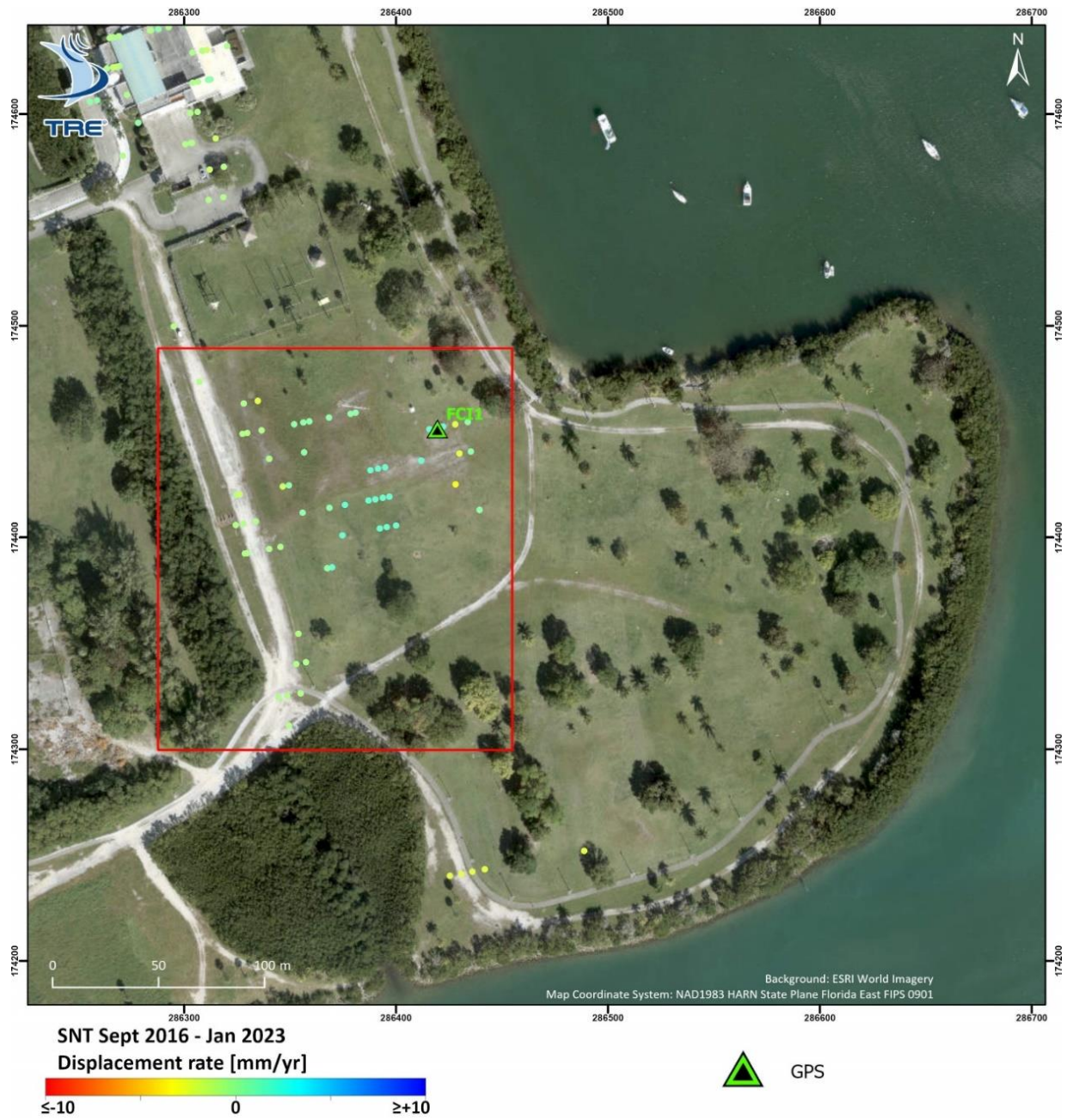


Figure 15: InSAR data selected (red box) near FC11.

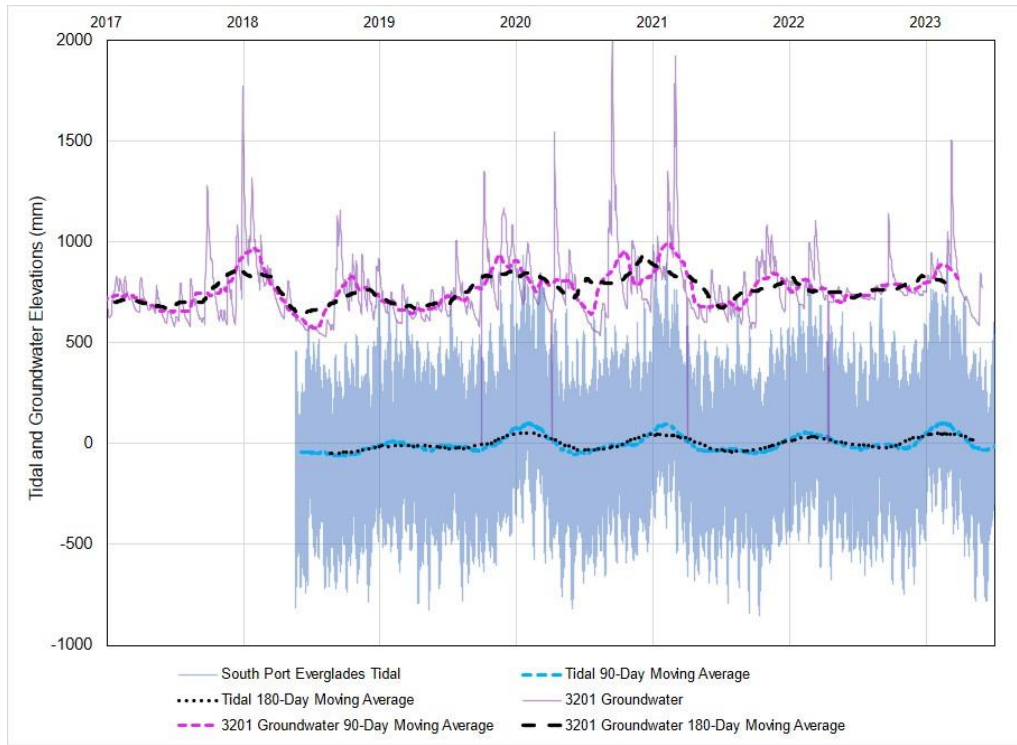


Figure 16: Comparison of groundwater and tidal data near FCI1.

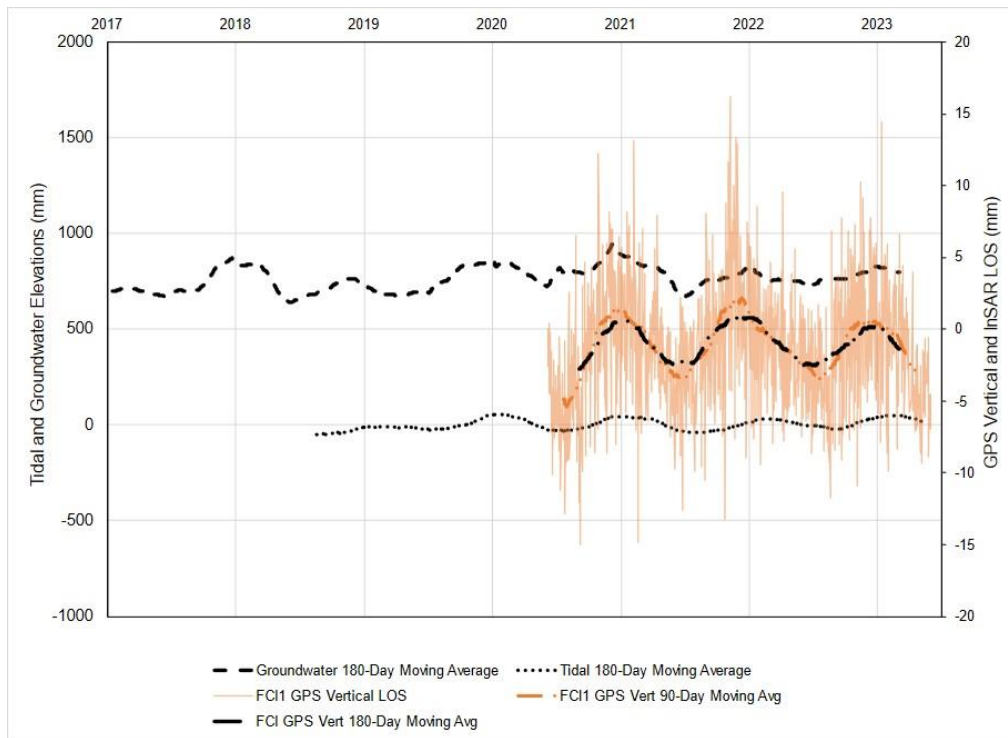


Figure 17: Comparison of FCI1 vertical component and nearby groundwater and tidal data

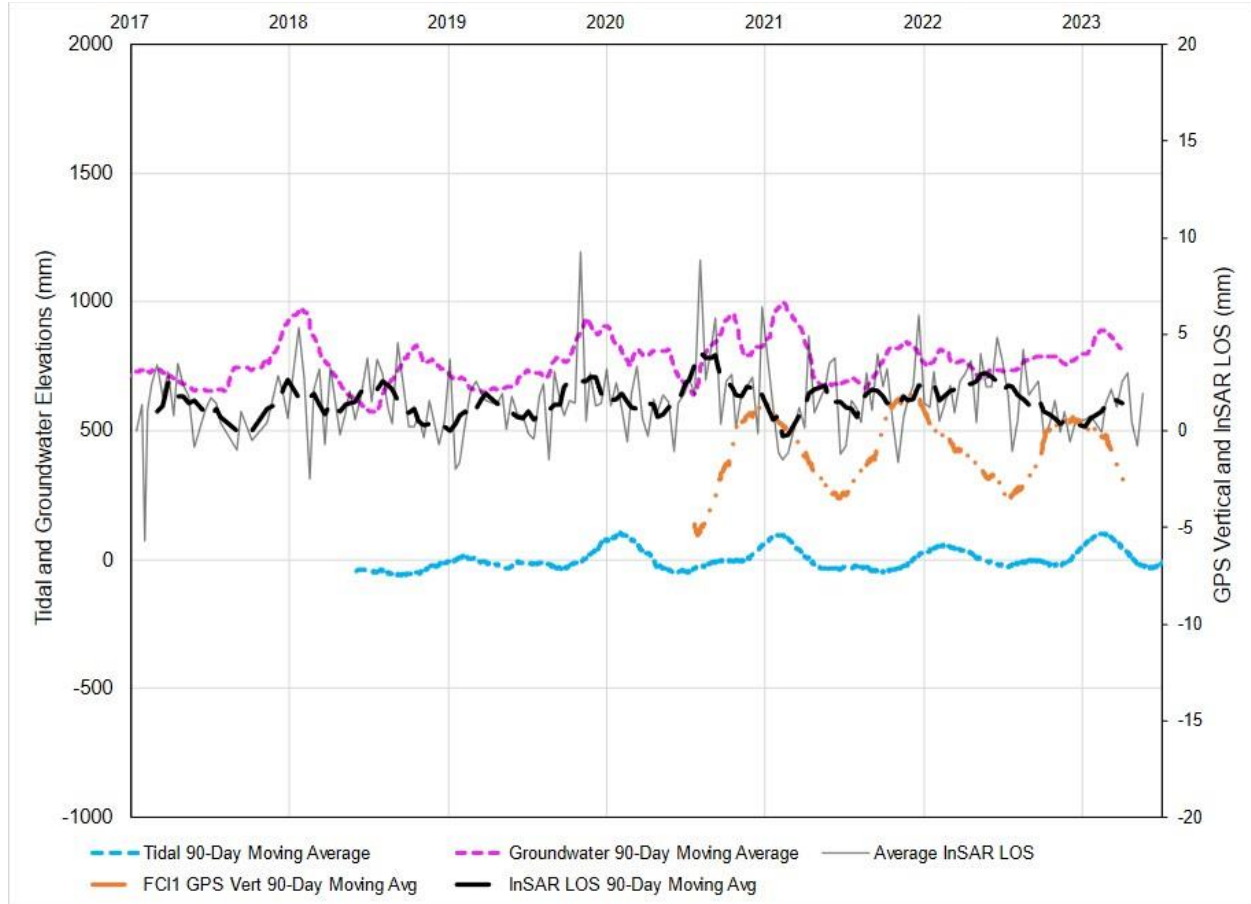


Figure 18: Comparison of average InSAR time series (SNT) against FCI1 vertical component and nearby groundwater data

5.2.1.2. Data validation at GPS Station FLMB

GPS station FLMB was selected for validation of the SNT InSAR time series as it is located within a geologic coastal area, and it is likely affected by tidal fluctuations. The area of FLMB also does not appear to have been altered by anthropogenic activity over the period of study and is well covered by InSAR measurement points (Figure 19).

The FLMB time series was compared against data from the Virginia Key, FL tidal gauge (approximately 6 km to the South). As described for station FCI1, the FLMB vertical time series data (adjusted to reflect the LOS direction) is correlated with the tidal data (with a correlation coefficient of approximately 0.5, considering 180-day moving average consistent with the semi-annual seasonal tidal fluctuations), likely due to its proximity to the coast. However, the average SNT InSAR displacement time series for the selected data (for points identified within the area of the FLMB station in Figure 19) does not exhibit a clear seasonal trend

visible in the groundwater and GPS time series and its fluctuations (Figure 20) are well within the error of the InSAR time series (i.e. displacement rate less than ± 1 mm/yr and amplitude of the time series less than the average ± 3.5 mm error-bar, Table 5).

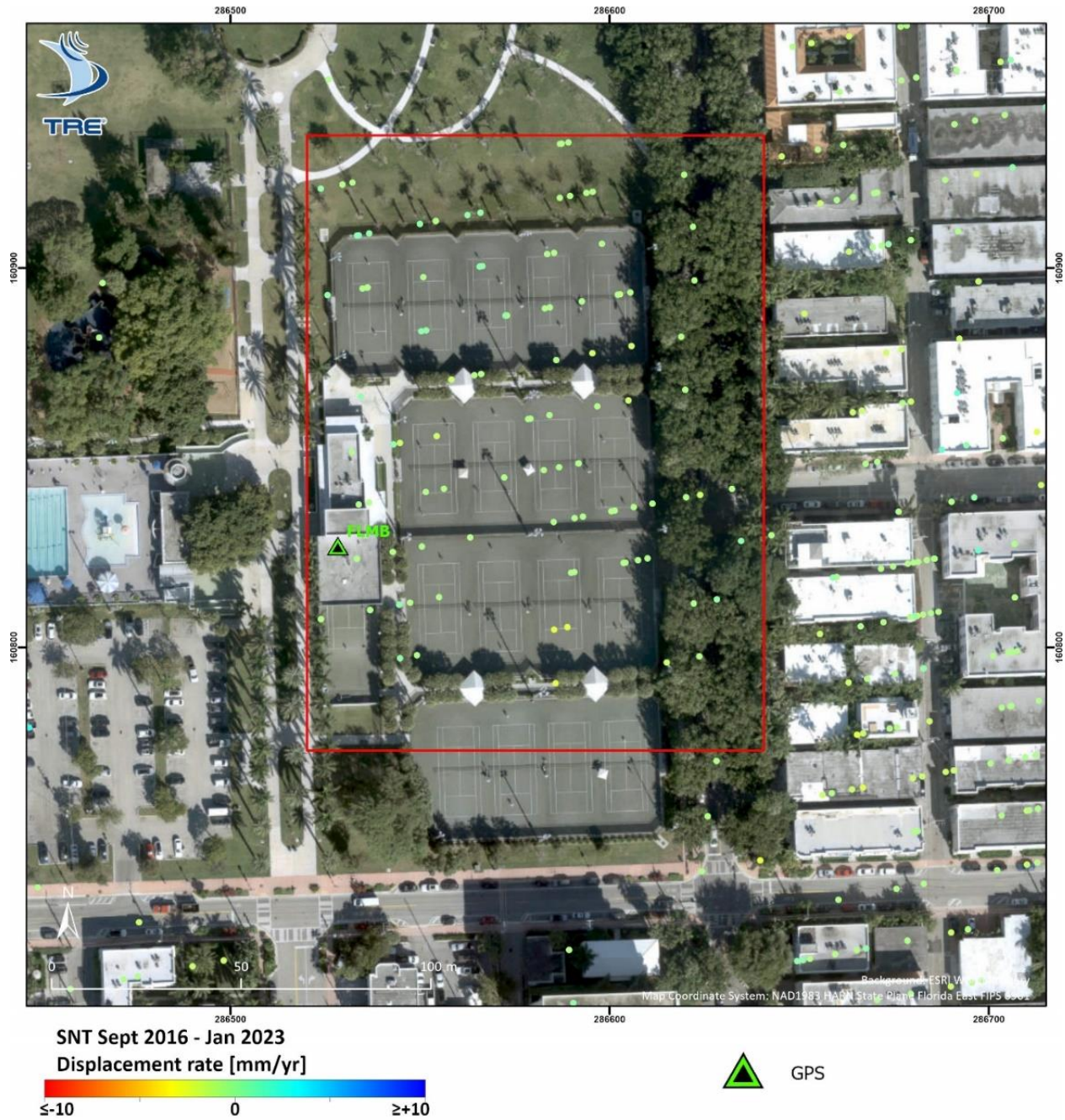


Figure 19: InSAR data selected (red box) near FLMB.

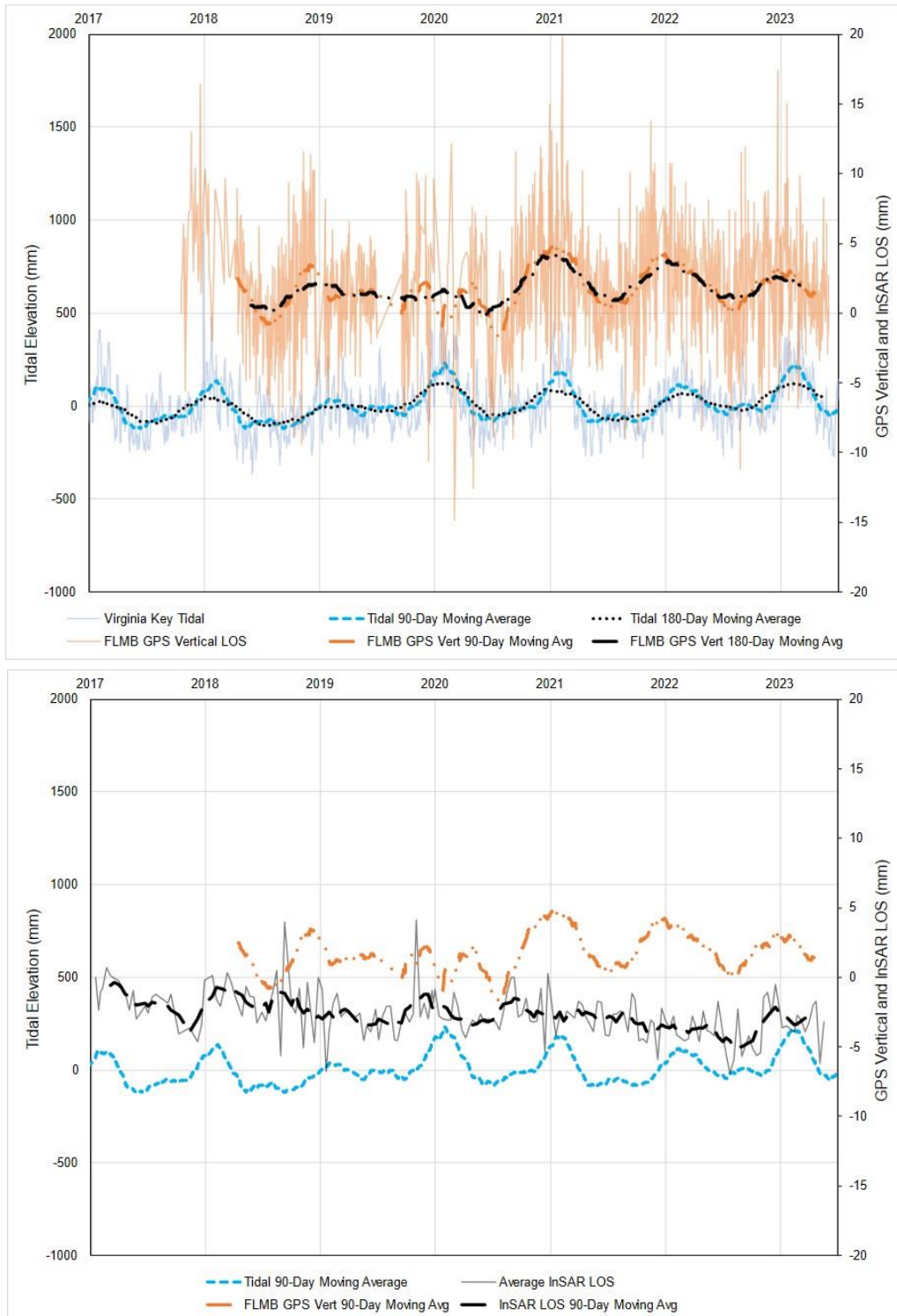


Figure 20: FLMB vertical component and near-by tidal data (up) and comparison of their average trends with the average InSAR time series (below)

5.2.1.3. Data validation at GPS Station ZMA1

GPS station ZMA1 was selected for ground truthing of the SNT InSAR time series because it is located in an inland area affected by seasonal groundwater fluctuations, it has the best temporal coverage over the period of study from all of the considered GPS stations, the area does not appear to have been altered by anthropogenic activity over the period of study, and is well covered by InSAR measurement points (Figure 21).

ZMA1 was compared against data from groundwater monitoring well numbers 254950080180801 and 254832080175001 (each within approximately 2.5 km). As illustrated in Figure 22, the ZMA1 vertical time series data (adjusted to reflect the LOS direction) has an overall negative linear trend and is correlated with the short period seasonal fluctuations (90 day averaged) of the groundwater level (correlation coefficient of approximately 0.4). The average SNT InSAR displacement time series for the selected data (for points identified within the area of the ZMA1 station in Figure 21) exhibits a seasonal trend though it is within the error of the displacement time series. The negative trend in the average InSAR time series data for the selected points around station ZMA1 appears to be relatively correlated with the groundwater data, despite a correlation coefficient of approximately 0.1 (a reliable correlation with the groundwater and GPS timeseries data cannot be calculated due to the relative noise. As discussed earlier, seasonal fluctuations below the precision of the InSAR time series cannot be detected, as well as fluctuations affecting the whole Local AOI.



Figure 21: InSAR data selected (red box) near ZMA1.

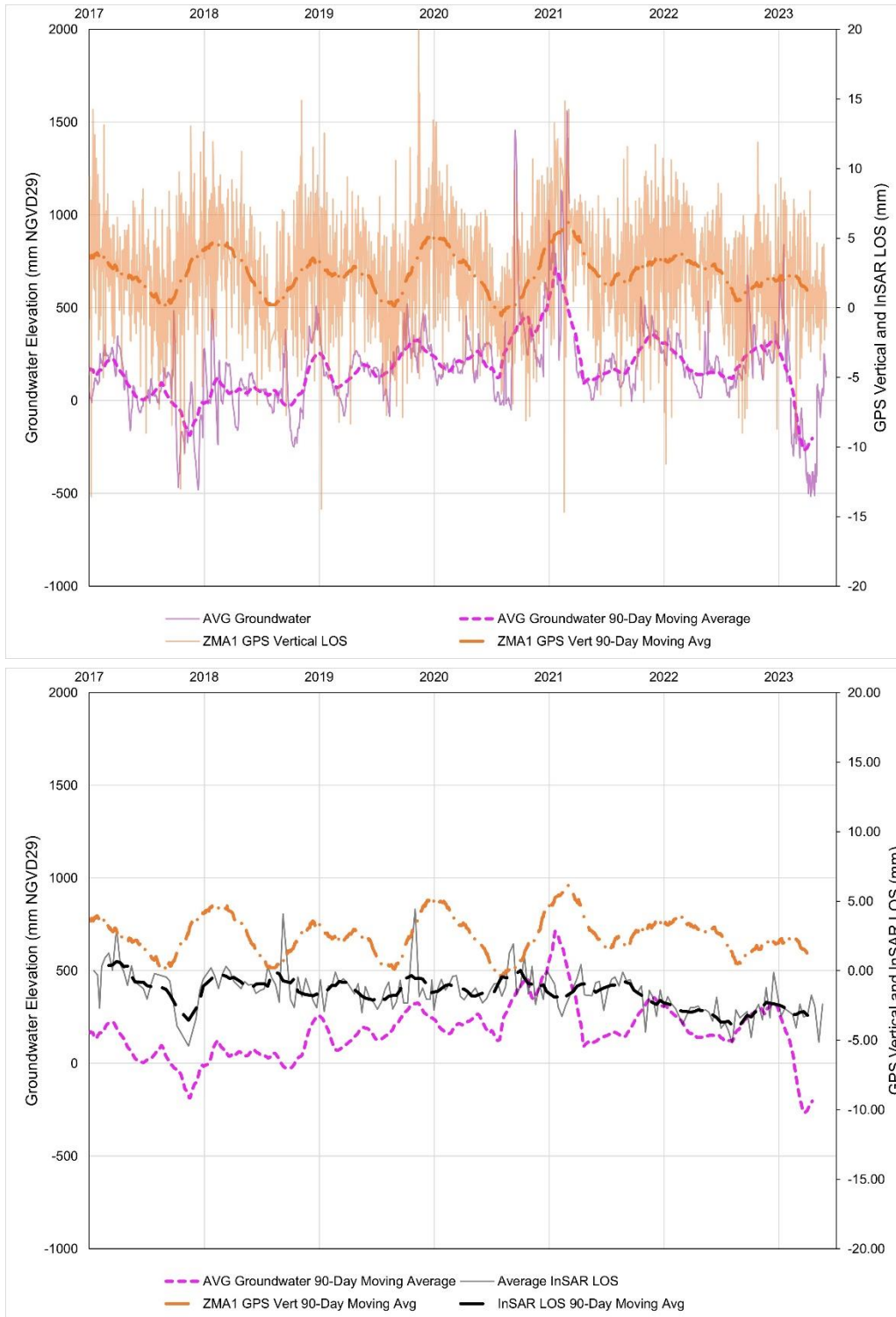


Figure 22: ZMA1 vertical component and near-by groundwater data (up) and comparison of their average trends with the average InSAR time series.

5.2.2. Potential Sources of Error

Understanding the potential sources of error and uncertainty related to interpretation of InSAR time series data is crucial to the process of identifying both spatial and temporal trends within the data. The main potential source of error is due to an attempt to compare spatial and temporal trends that are beyond the capabilities of InSAR technology. In particular:

- Measuring displacements in areas that are smaller than the resolution of the satellite (i.e. 5 m x 20 m pixel size with SNT) is not possible. To identify movement, InSAR requires an area covering at least a few pixels of the SAR image and that remains consistent over at least a few consecutive images (i.e., the displacement signal overcomes the intrinsic noise of single acquisitions). Even when using advanced InSAR techniques such as SqueeSAR, if the movement involves one single pixel (i.e., one single measurement point) it is only possible to accurately measure a displacement within $\pm\lambda/4$ (± 1.4 mm using C-band SNT data) between two consecutive images (see Section 3.2.2 for details). Rapid movements (i.e., larger than this theoretical limit) can be detected if the deforming area involves at least a few pixels or a cluster of measurement points. Additionally, in the case of just a single point, its location accuracy is on the order of meters and depends on the satellite resolution.
- Sources of noise in InSAR measurements have been discussed in Section 3 but it is worth remarking that single displacement measurements within the time series can be affected by residual atmospheric or decorrelation noise even when processed with advanced InSAR techniques such as SqueeSAR. Possible single jumps in the displacement time series (i.e., a displacement step without a subsequent increase of displacement rate) or minimal trend changes (i.e., within the error bar of the displacement rates) should be evaluated based on the precision of the measurements obtained with each processed dataset. Average precision values are reported in Table 5, but every point is delivered with a specific set of precision parameters. If the displacement is within ± 2 sigma of the time series error bar value (STD_DEF) or the displacement trend is within ± 2 sigma of the average displacement rate standard deviation (V_STDEV), the point may not be statistically relevant.
- To a similar extent, measurement point time series are sensitive to surface changes, such as those that occur during construction activities. Areas and periods of lower coherence and/or decorrelation may affect the time series of displacement. In these cases, it is important to consider that the interpretation of displacement trends that are not consistent for at least 4 to 5 consecutive images are most likely not reliable.
- Measurement point location accuracy has been discussed in section 3.2.2.2 but it is worth remarking that the location accuracy of SNT measurement points is in the order of ± 8 m in the NS direction, ± 12 m in the EW direction and ± 8 m in the vertical direction. For this reason, SNT data is not suitable for

the analysis of single buildings or infrastructures, such as residential structures that are the size of a few pixels but should be used only for the analysis of wide area trends.

- Finally, it is noted that all measurements provided by this study are 1-D Line Of Sight (LOS) measurements because of the absence of historical data acquired over the site in double orbit (i.e., ascending and descending) in overlapping periods. Interpreting LOS displacement as vertical displacement requires the assumption of negligible horizontal components of the real displacement vector. If this assumption is not verified, the vertical estimation can be affected by a bias.

5.3. Analysis of displacement trends

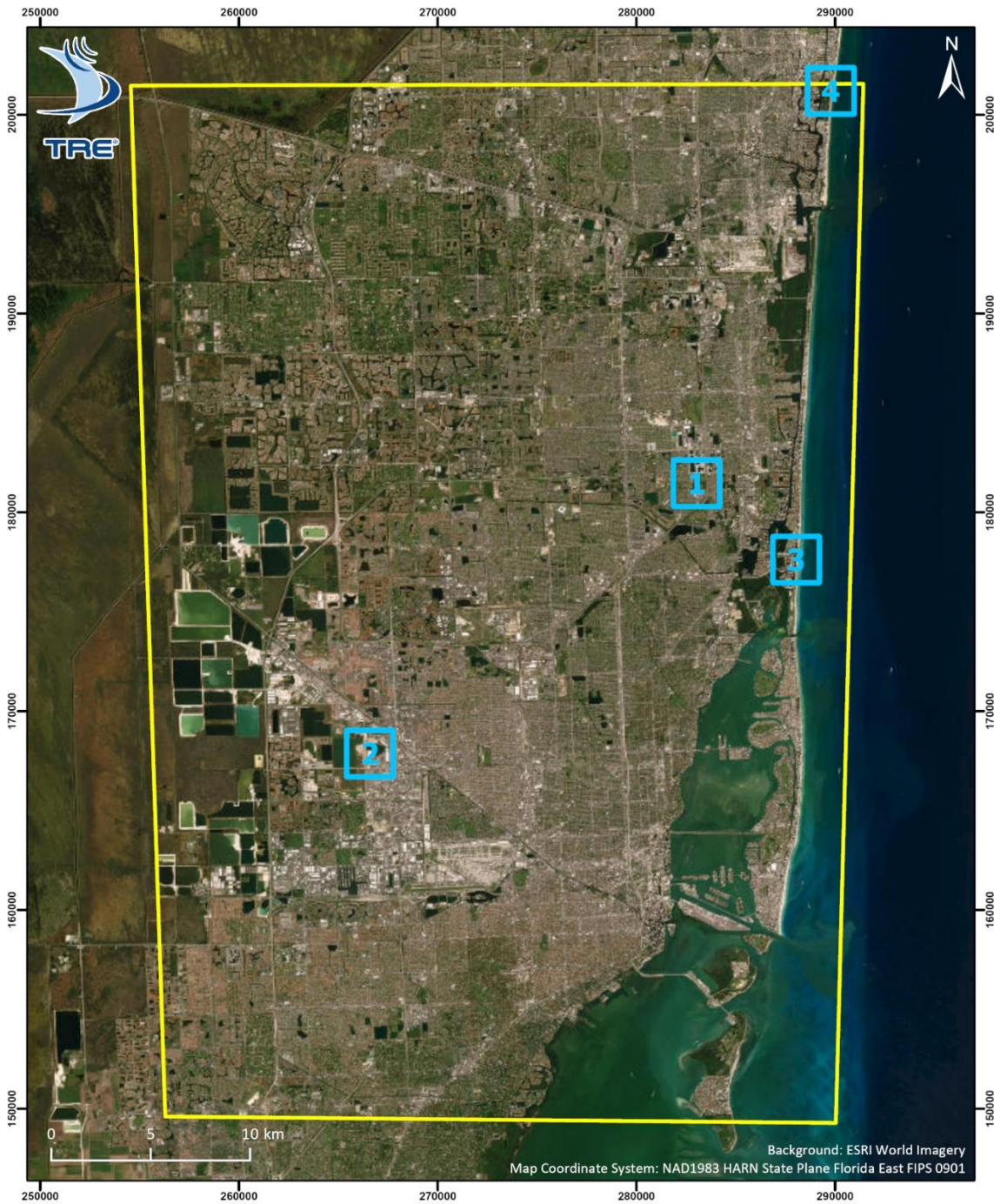
The analysis of the InSAR results has the main objective of identifying regional displacement trends. To this scope, cumulative displacement, displacement rate, acceleration and seasonality maps (from Figure 10 to Figure 12) were analyzed in combination with the transects defined by NIST (Figure 13) and covering a majority of the AOI.

The maps and longitudinal profiles of displacement rate along the transects (all reported in Appendix 1) confirm that there is no evidence of wide-area subsidence phenomena.

Despite the absence of wide-area displacement trends, localized areas of displacement over the study area can be identified in the InSAR results. Taking all limitations into account (as detailed in section 5.2.2), such as the low satellite resolution, the low accuracy of the point location and the precision of the measurements, areas of displacement may be identified by looking at clusters of points with a displacement rate greater than the precision of the measurements (at least ± 2 mm/yr, which corresponds to ± 2 sigma of the average standard deviation) and/or non-linear trends. Examples of some localized areas of displacement within the AOI are listed in Table 10, reported in Figure 23 and described in the following Sections. These sites should be interpreted as examples of localized areas of displacement but were not investigated or visited as part of this study. Additional site-specific investigations would be required to confirm the trends identified in the InSAR data and verify the possible source of surface displacement.

Table 10: Examples of localized areas of displacement.

#Area	Latitude	Longitude	Description
1	25.969161°	-80.170883°	Localized settlement
2	25.847321°	-80.335732°	Fill settlement and recent construction
3	25.934215°	-80.121112°	Construction settlement
4	26.146881°	-80.102041°	Coastal subsidence



 Area of Interest (AOI)

 Localized area of displacement

Figure 23: Location of localized areas of displacement selected as examples within the AOI.

5.3.1. Localized ground settlement

One example of localized ground settlement was identified within the Ives Estates Park area (Area 1 in Figure 23). A review of historical aerial imagery suggests that the site was developed between 1995 and 1999. Prior to development, the site was densely vegetated.

As illustrated in Figure 24, a cluster of points over a grassy part of a field is clearly exhibiting progressive displacement (average LOS displacement rate of approximately 9.3 mm/yr). It is noted that the presence of vegetation on the ground is a source of noise for InSAR data (as detailed in Section 3.2) and may be the cause of the absence of measurement points over most of the field.

Historical site use may suggest that the settlement observed over that cluster is due to the local geology¹¹ but recent optical images also suggest recent construction and possible fill settlement. Additional investigations, which are out of scope for the current study, are required to clarify the nature of the displacement and verify the real extent of the movement over the grassy areas where InSAR measurement points were not identified.

¹¹ Approximately 1 km to the southeast (Lat: 25.96256 deg; Lon: -80.16641 deg), the Florida Department of Environmental Protection records indicate that a sinkhole (reference number 87-001) occurred on 22 August 1972

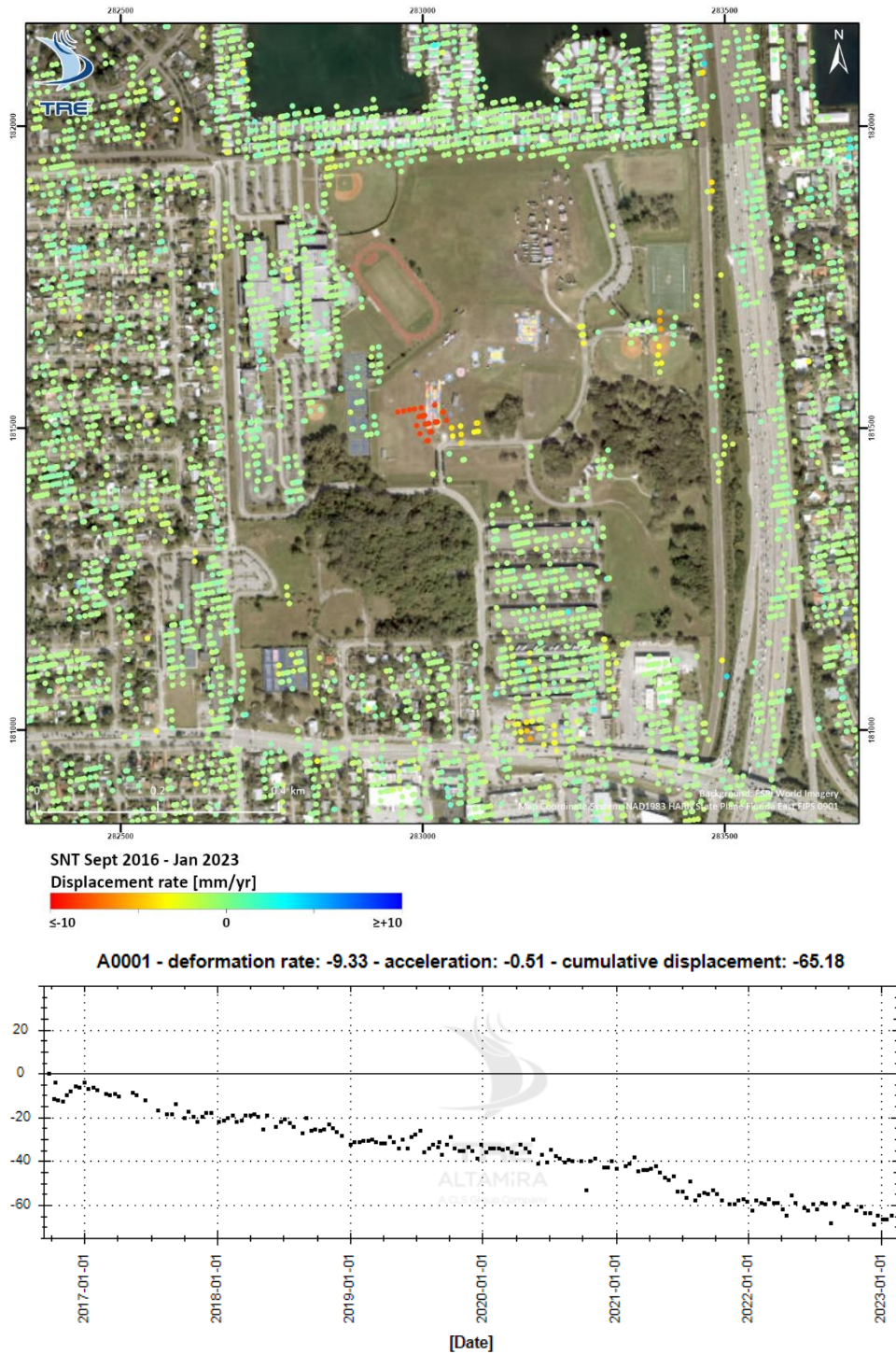


Figure 24: Area1 of ground settlement observed within the Local AOI. The average time series (ATS) of the points with the highest displacement rates is also visualized to characterize the displacement trend. The graph indicates the displacement [mm] over time and the legend reports the average displacement rate [mm/yr], acceleration [mm/yr²] and cumulative displacement [mm].

5.3.2. Ground settlement associated with anthropogenic fill

One example of a visible displacement trend is along transect T2 (Figure 25) at approximate Station 5, where a short stretch of negative velocities is measured.

At this location (Area 2 in Figure 23), several north-south trending structures (likely industrial) were observed to be settling at an average LOS displacement rate of approximately 3 mm/year (Figure 26). A review of aerial imagery of the site reveals that these structures (which were constructed between 2016 and 2017) are built over man-made fill which was progressively developed since at least 1994. Depending on the characteristics of the man-made fill and structures constructed upon them, settlement can be a common occurrence. Other instances of settlement of man-made fill may explain similar settlement rates in other areas of displacement within the AOI.

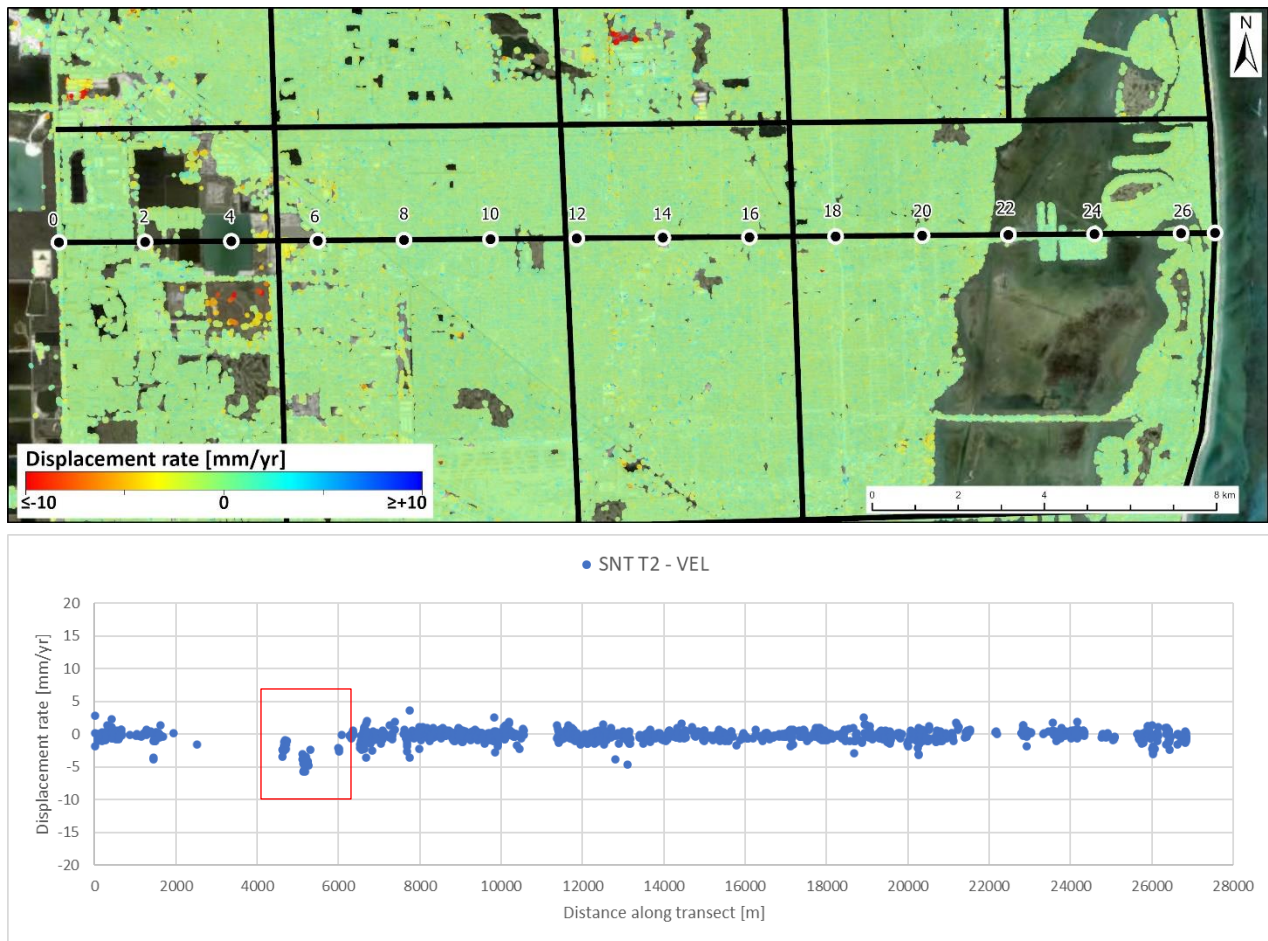
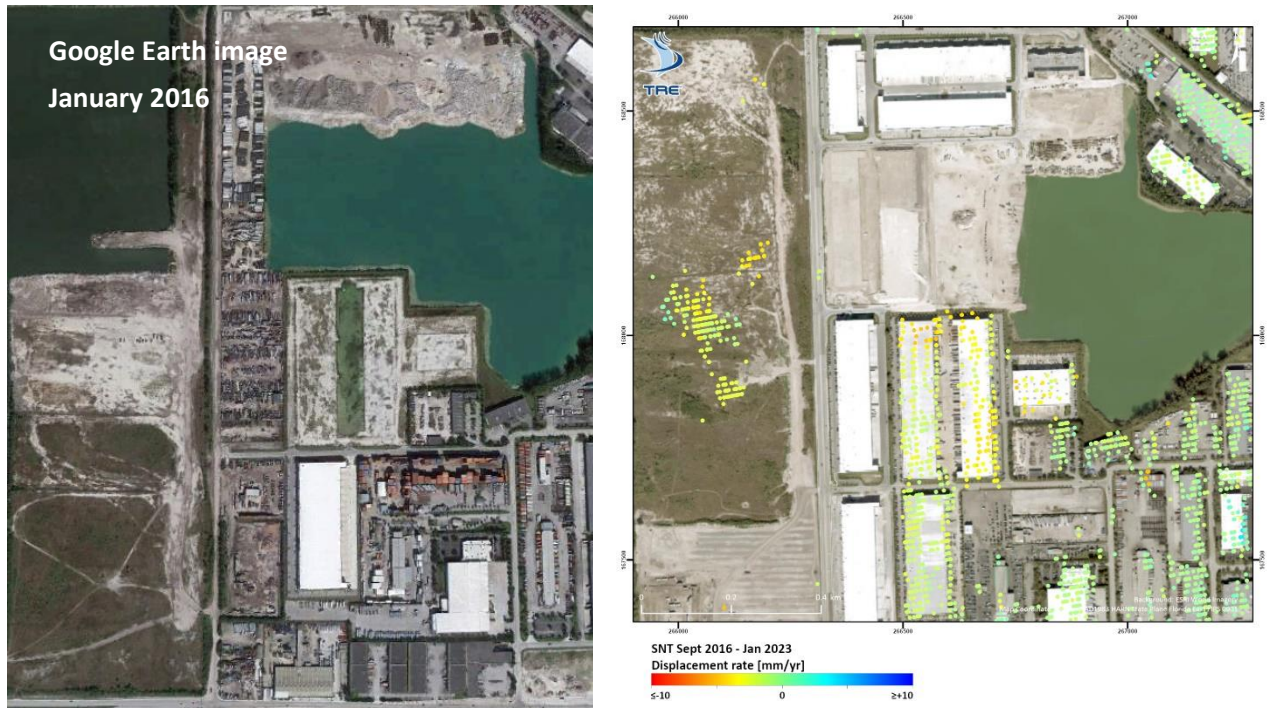


Figure 25: SNT transect T2, reporting the displacement rates of the measurement points identified within a 10-m buffer from the profile. The localized area of displacement is highlighted with the red box.



A0001 - deformation rate: -2.98 - acceleration: -0.12 - cumulative displacement: -17.45

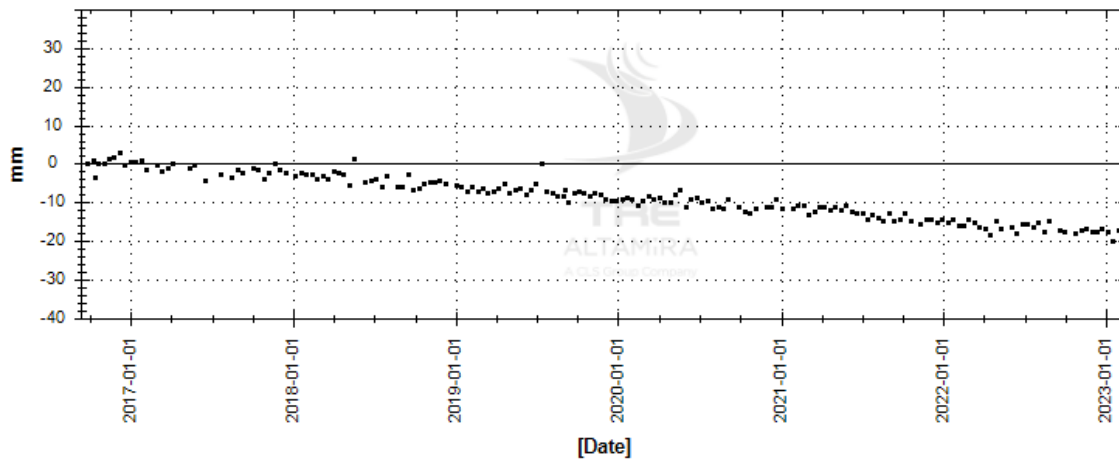


Figure 26: Building settlement likely associated with construction over fill at Area 2. The average time series (ATS) of the points identified over the industrial structures is also visualized to characterize the displacement trend. The graph indicates the displacement [mm] over time and the legend reports the average displacement rate [mm/yr], acceleration [mm/yr²] and cumulative displacement [mm]. The top left image is from Google Earth and shows the area in January 2017.

5.3.3. Ground settlement due to coastal development

A second example of active ground displacement related to new construction can be observed along the east coast of the AOI (Section TE between Station 10 and Station 16, Figure 27). In this area, a review of aerial photographs shows that several high-rise structures have been recently developed, and in some cases are still under development. In this specific case (Area 3, Figure 23), development of the site began circa 2007 with the construction of two structures and in 2016 two additional structures were developed (Figure 28). This area corresponds to the areas of negative InSAR velocity profiles shown in Section TE near Station 14.5. The ground displacement rates were highest in 2016 to 2020 (average LOS displacement rate of approximately 14 mm/yr) and slowed considerably since then, which is consistent with ground settlement conditions under new construction.

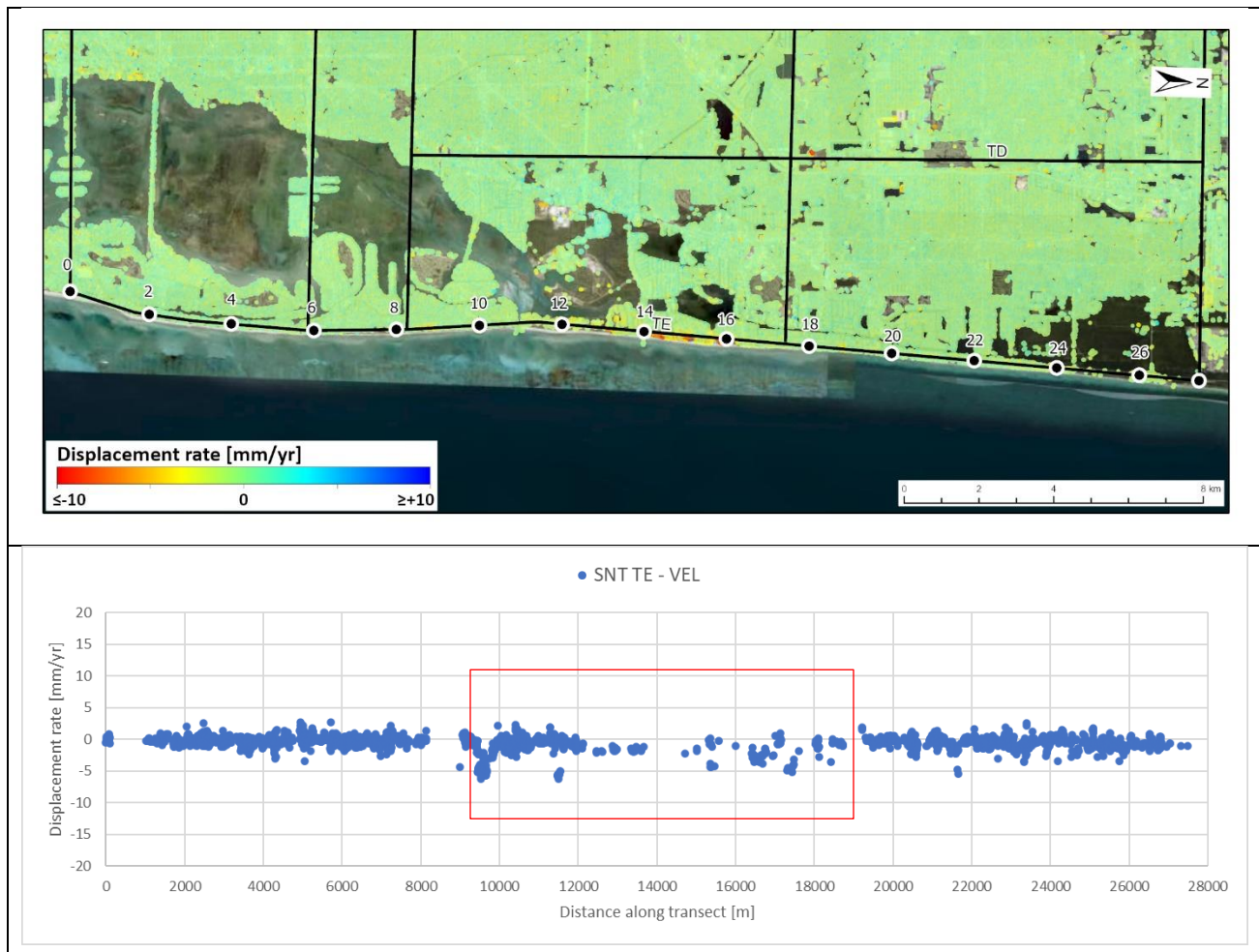


Figure 27: SNT transect TE. Localized areas of displacement are observed along the coast between Station 10 and 16 (red box on the profile).

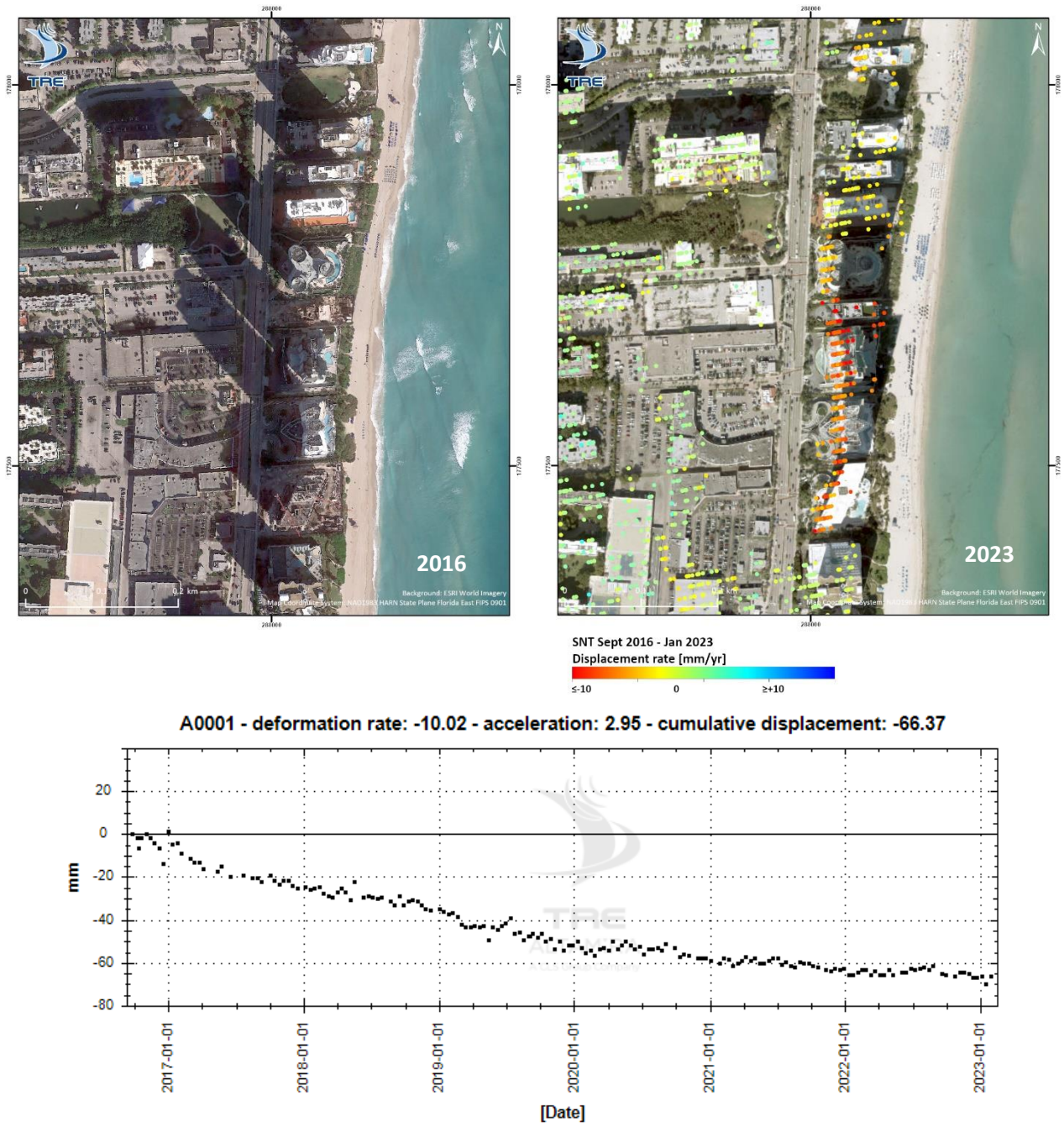


Figure 28: Building settlement due to recent construction at Area 3. An average time series (ATS) of points identified over some buildings is also visualized to characterize the displacement trend. The graph indicates the displacement [mm] over time and the legend reports the average displacement rate [mm/yr], acceleration [mm/yr²] and cumulative displacement [mm].

5.3.4. Coastal subsidence associated with changed conditions

A different type of ground subsidence was also observed along the coast (Figure 29), and specifically in an isolated area, in the northeast corner of the Local AOI (Area 4, Figure 23). Even if the average displacement rate is on the order of a few mm/yr, the area presents a common sudden trend acceleration in 2020.

This example of ground subsidence occurs in a neighborhood where aerial imagery suggests that no visible changes to the ground surface have occurred over the period of study. No groundwater or GPS data were located near this site, so the InSAR time series could not be “ground truthed” at this specific location. Additional site-specific investigations, out of scope for the current study, would be required to confirm the trends identified in the InSAR data and verify the possible source of surface displacement.

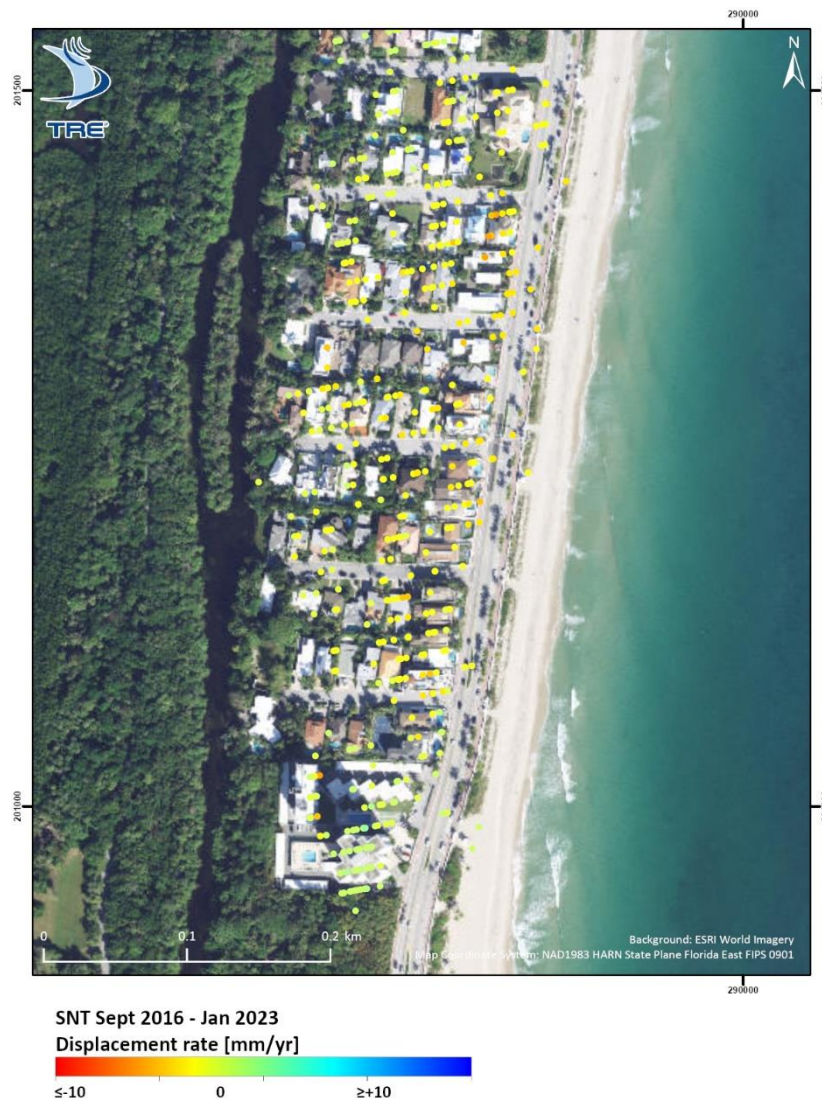


Figure 29: Coastal subsidence from changed conditions at Area 4..

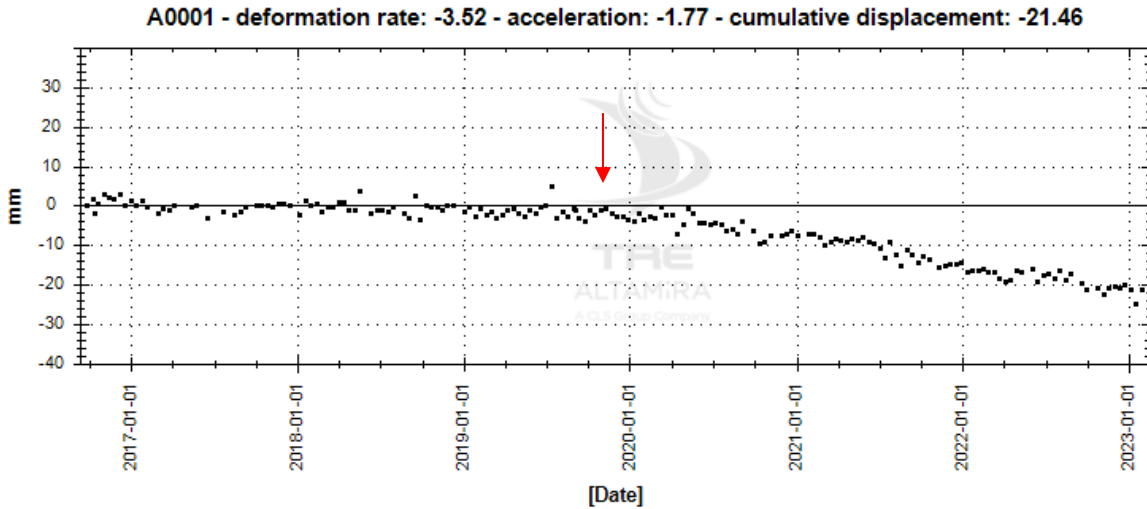


Figure 30: Coastal subsidence from changed conditions at Area 4. An average time series (ATS) of points identified in this area is visualized to characterize the common displacement trend. The graph indicates the displacement [mm] over time and the legend reports the average displacement rate [mm/yr], acceleration [mm/yr²] and cumulative displacement [mm]. The red arrow indicates approximately when the trend change started, at the end of 2019.

6. Conclusions

Based on the data analysis, the following main conclusions are provided:

- The analysis confirms that there is no evidence of wide-area subsidence, acceleration or seasonal trends affecting the area.
- However, the SNT results showed localized areas of ground surface displacement within the AOI. The majority of these areas could be interpreted as ground settlement processes resulting from recent building construction, compaction settlement of man-made fills, or as natural surface fluctuations due to hydrological conditions. However, the analysis of localized areas of displacement was out of scope for the current study and further investigations would be required to confirm the InSAR measurements and verify the source and extent of the surface displacement.

7. Appendix 1: Transects

Ten transects along the areas of interest (Figure 31) were defined and generated in accordance with NIST as follows:

- The transects include points within a ± 10 m buffer for the transect profile,
- Points within the buffer are projected to the profile without data interpolation or averaging, and
- The transects images report the annual displacement rate values (mm/yr) on the Y axis.

The transects are shown in the following Sections, using the World Imagery ESRI as background image.

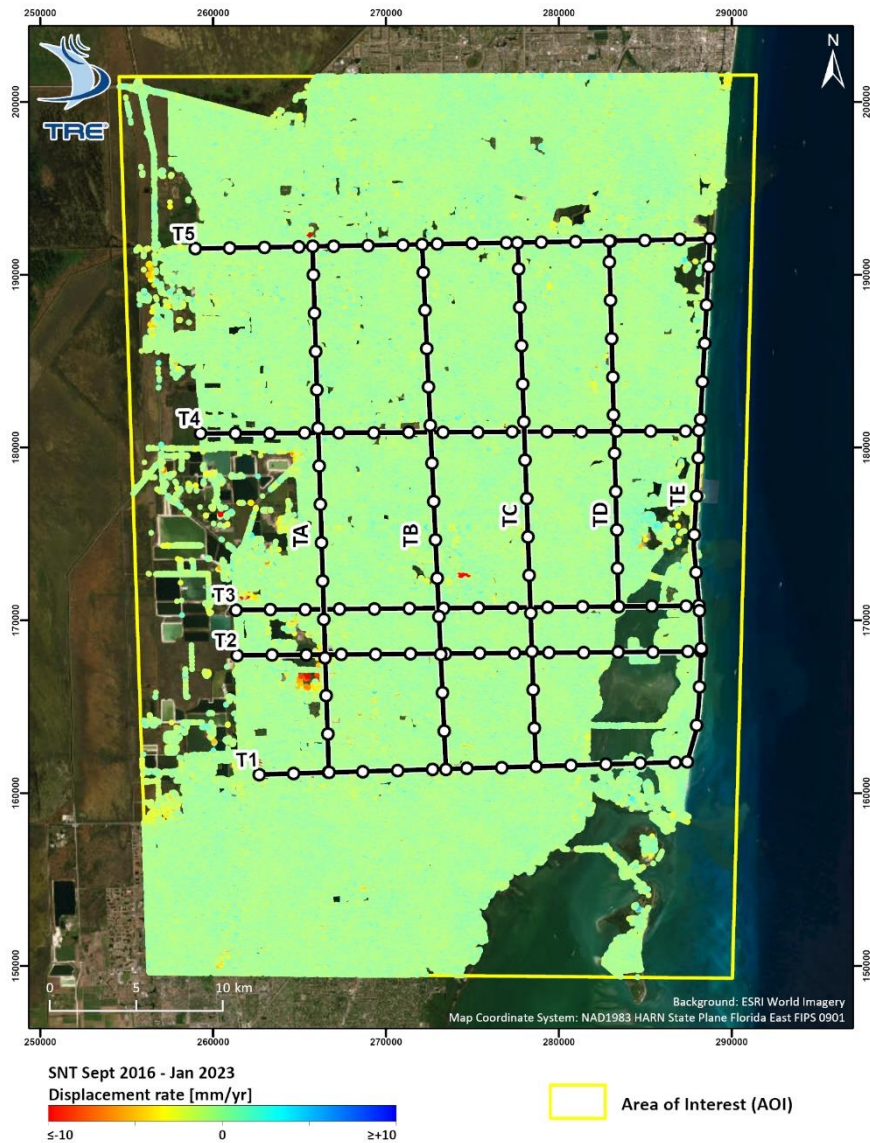
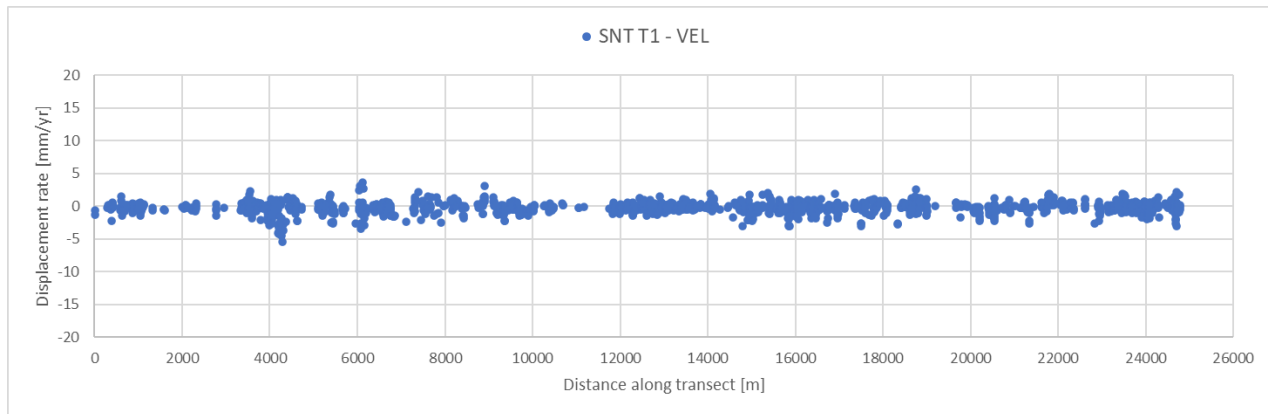
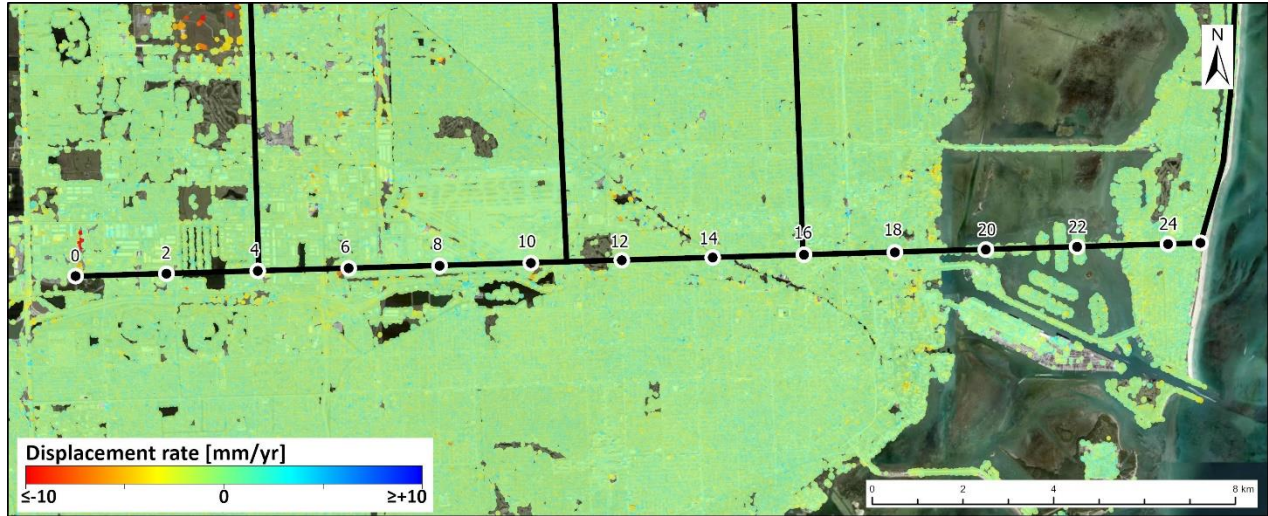
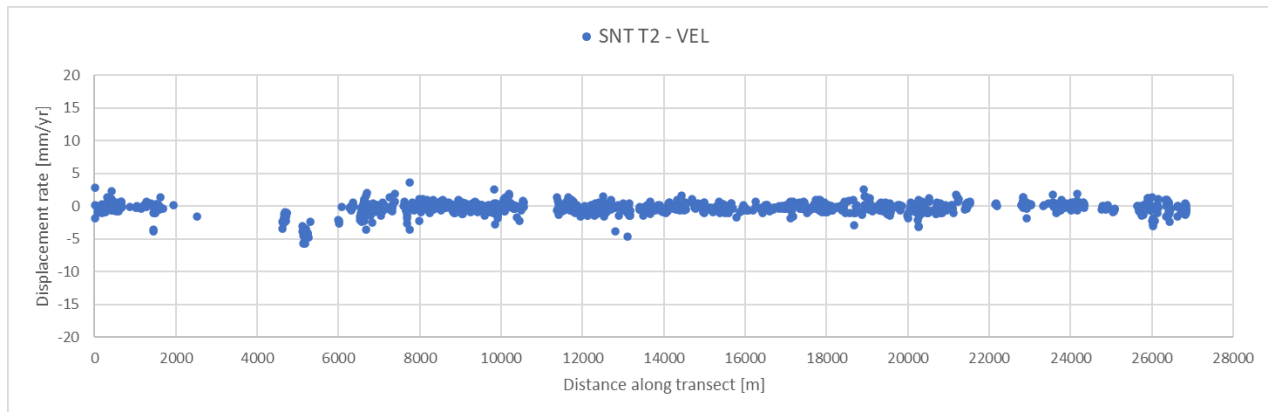
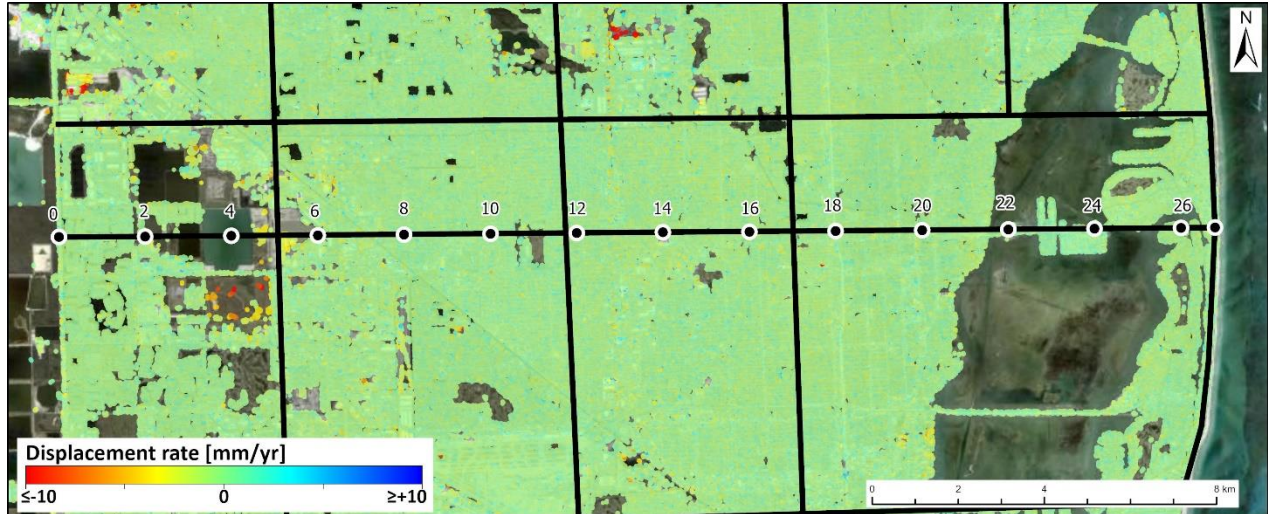


Figure 31: Location of the 10 Local area transects.

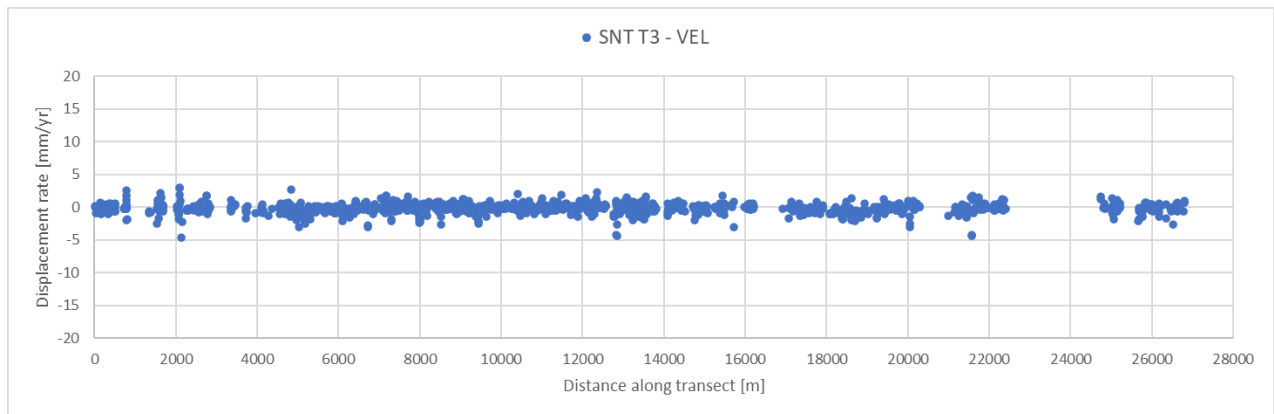
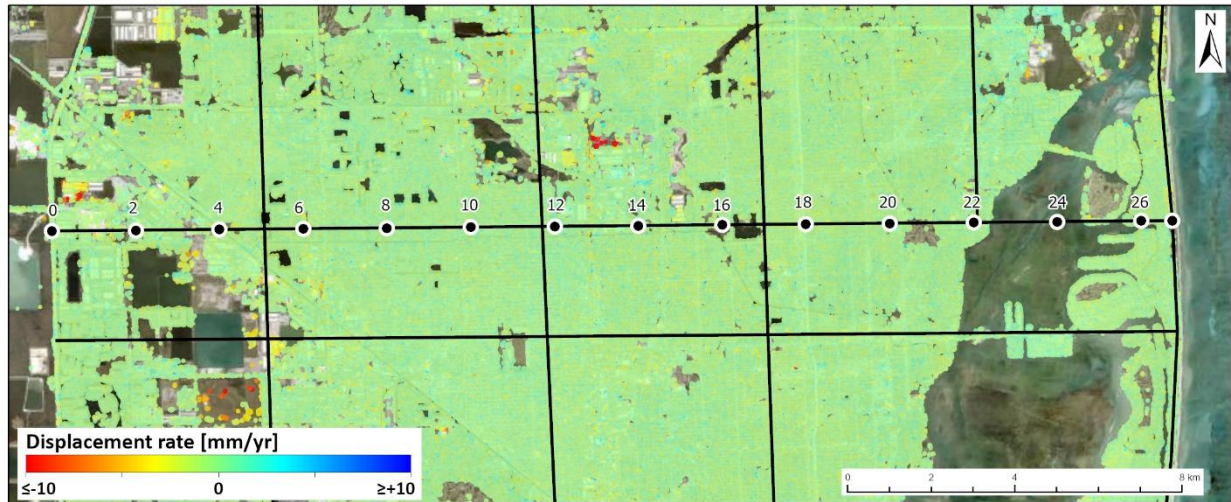
7.1. Local-SNT – T1



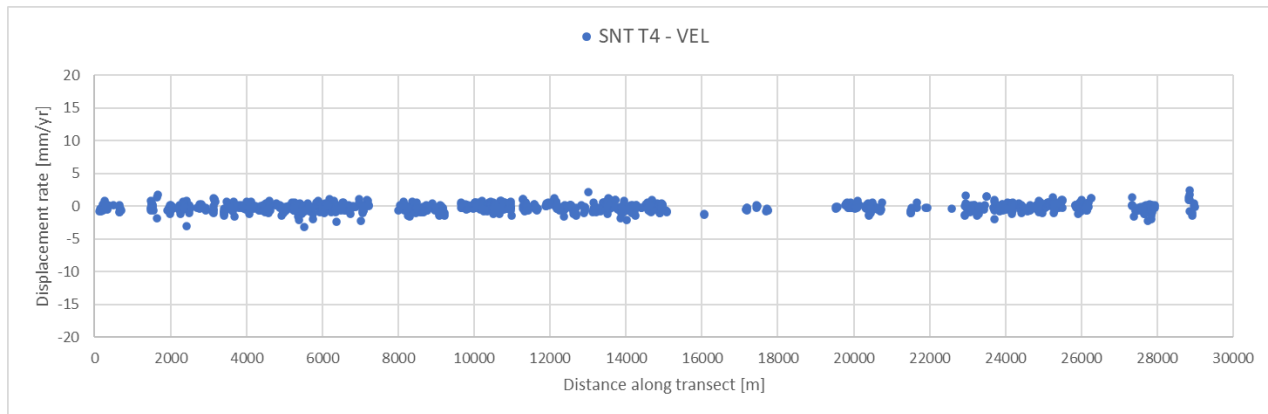
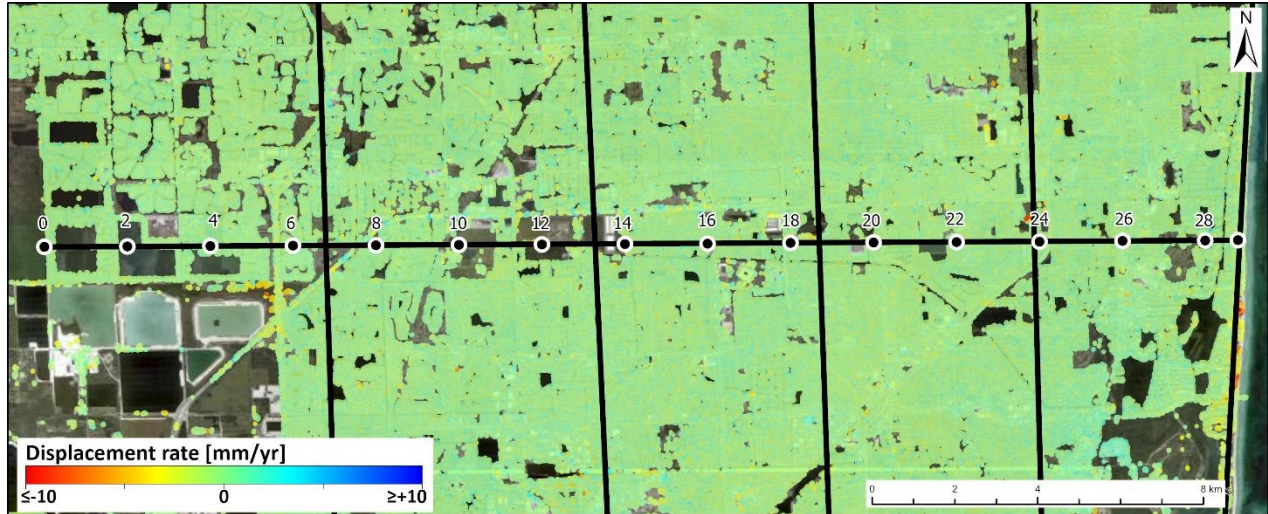
7.2. Local-SNT – T2



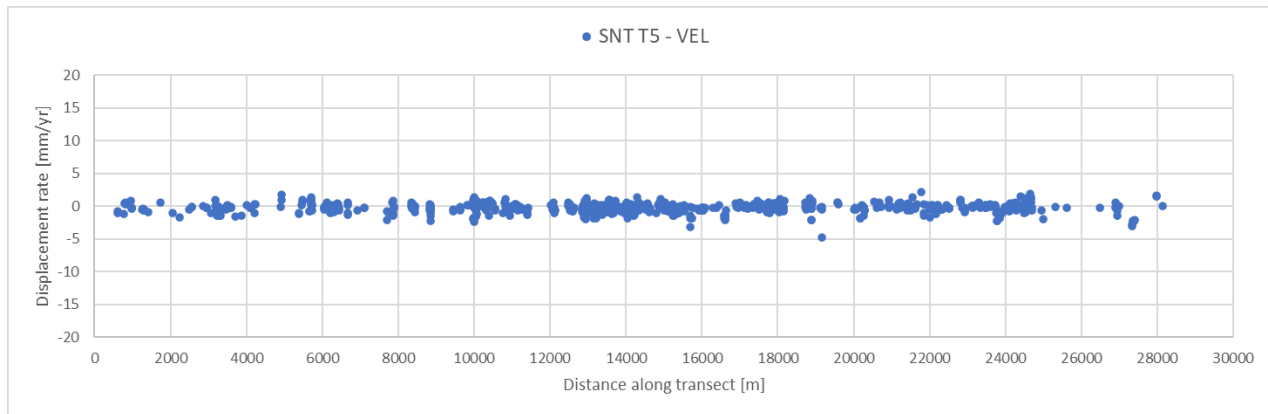
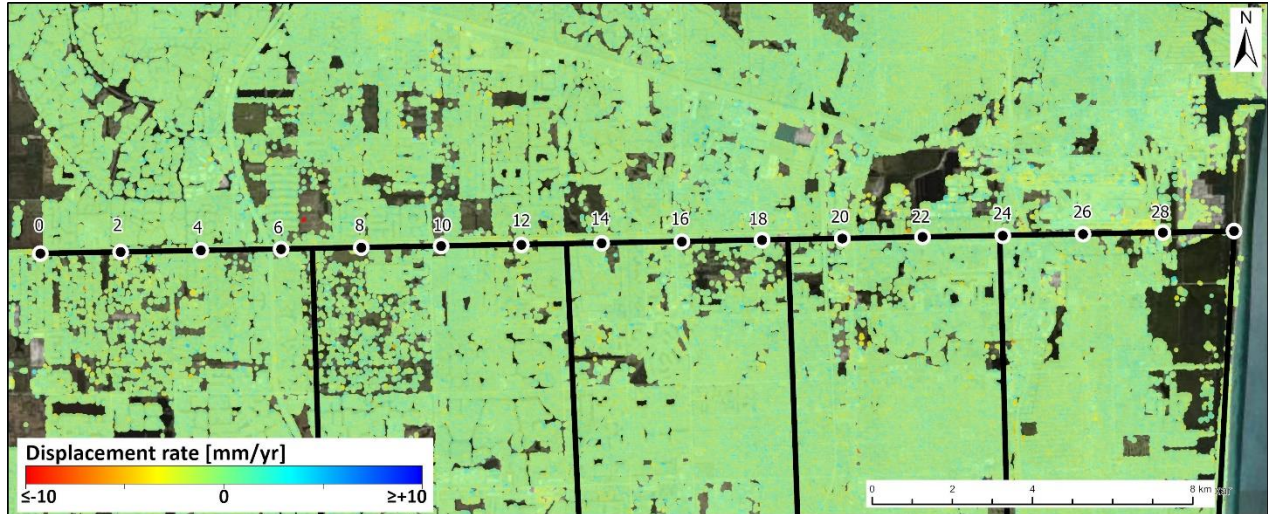
7.3. Local-SNT – T3



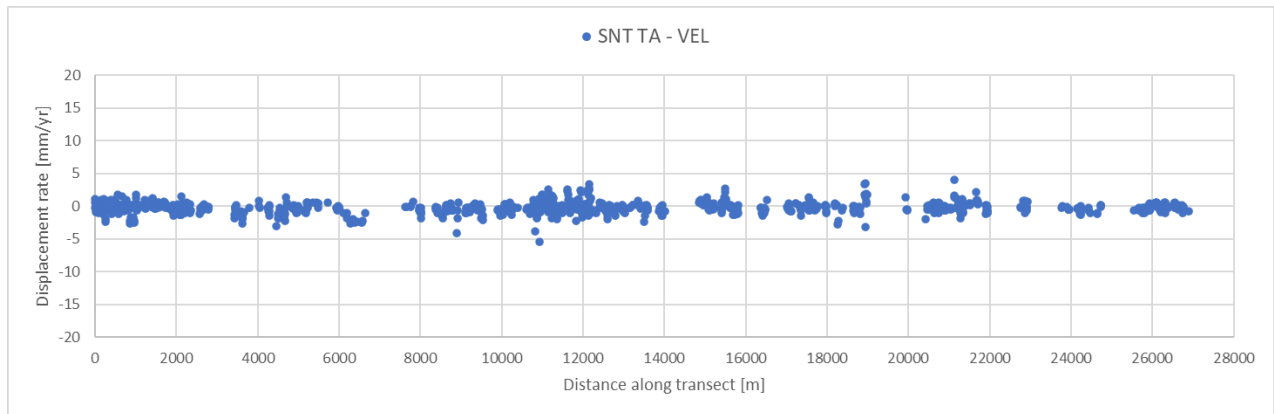
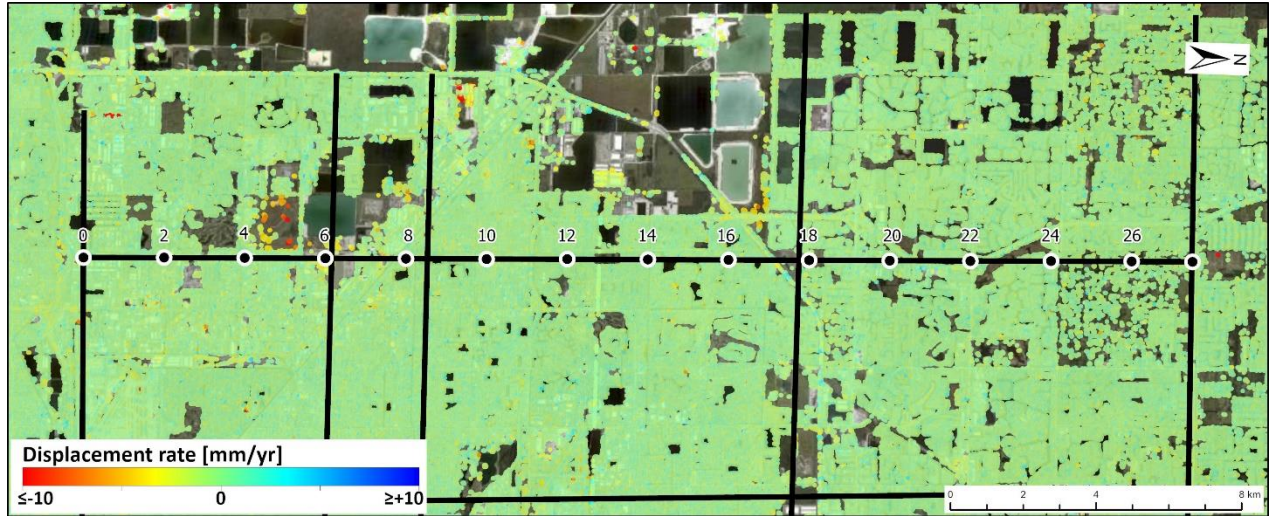
7.4. Local-SNT – T4



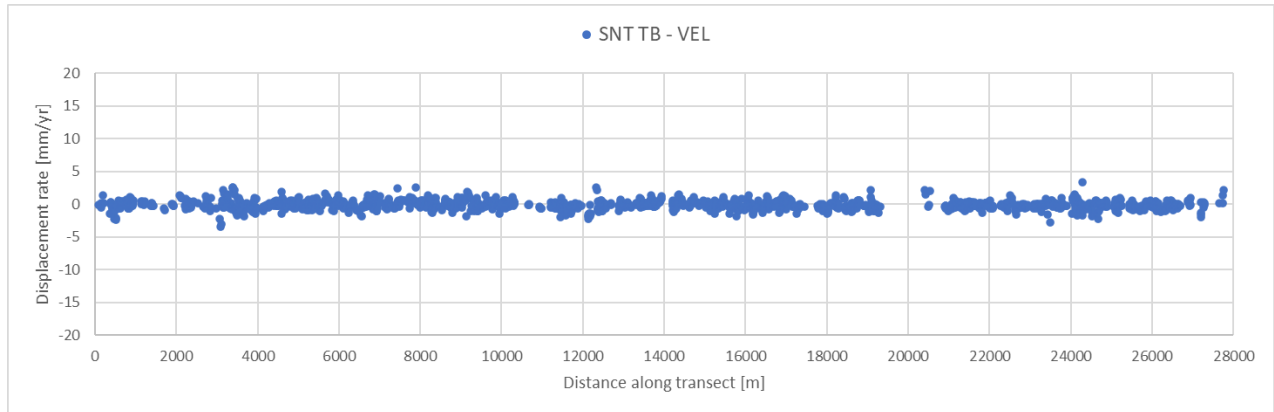
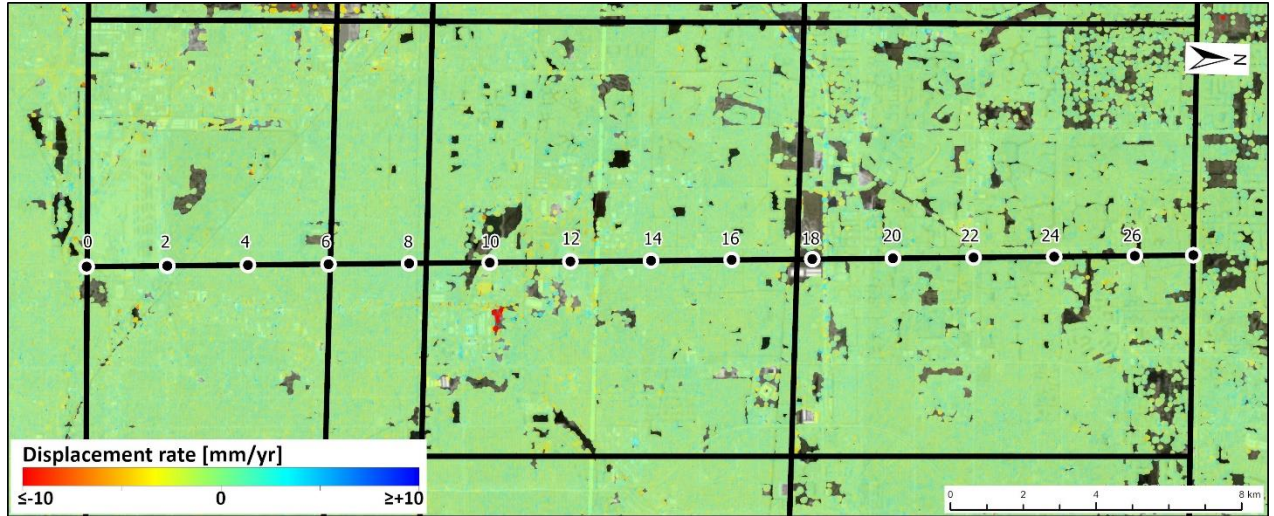
7.5. Local-SNT – T5



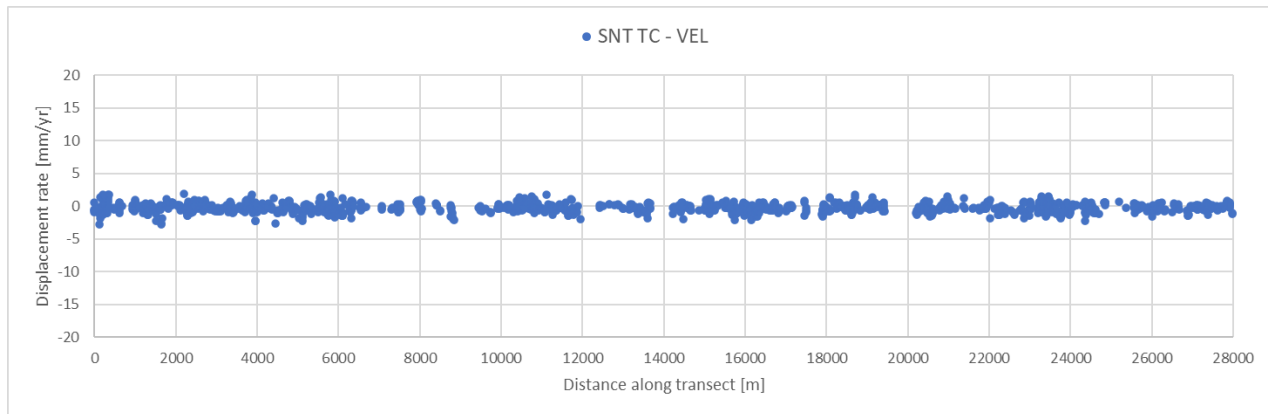
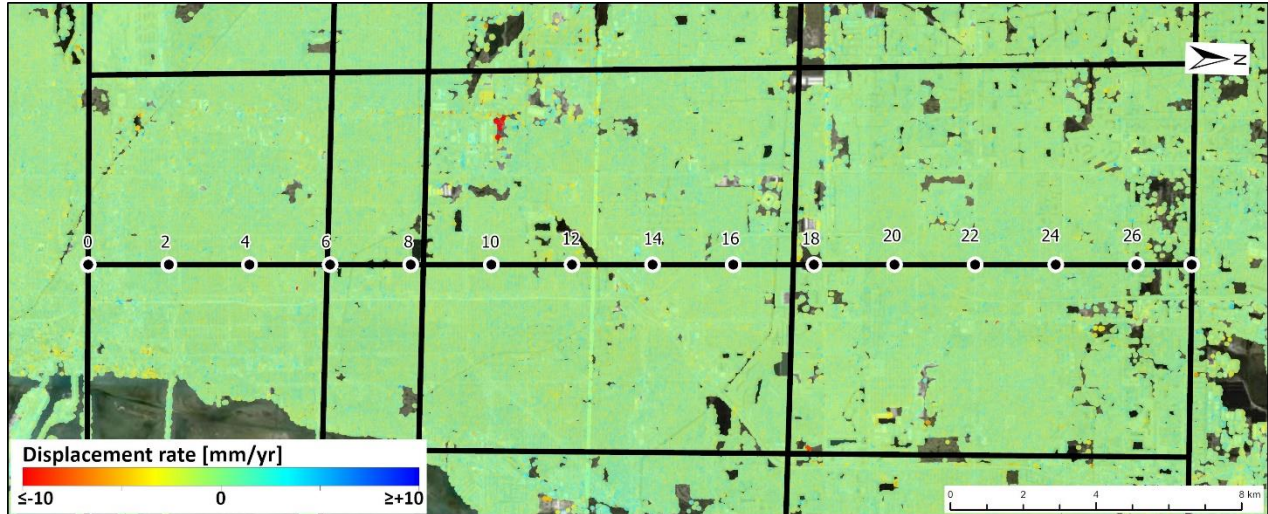
7.6. Local-SNT – TA



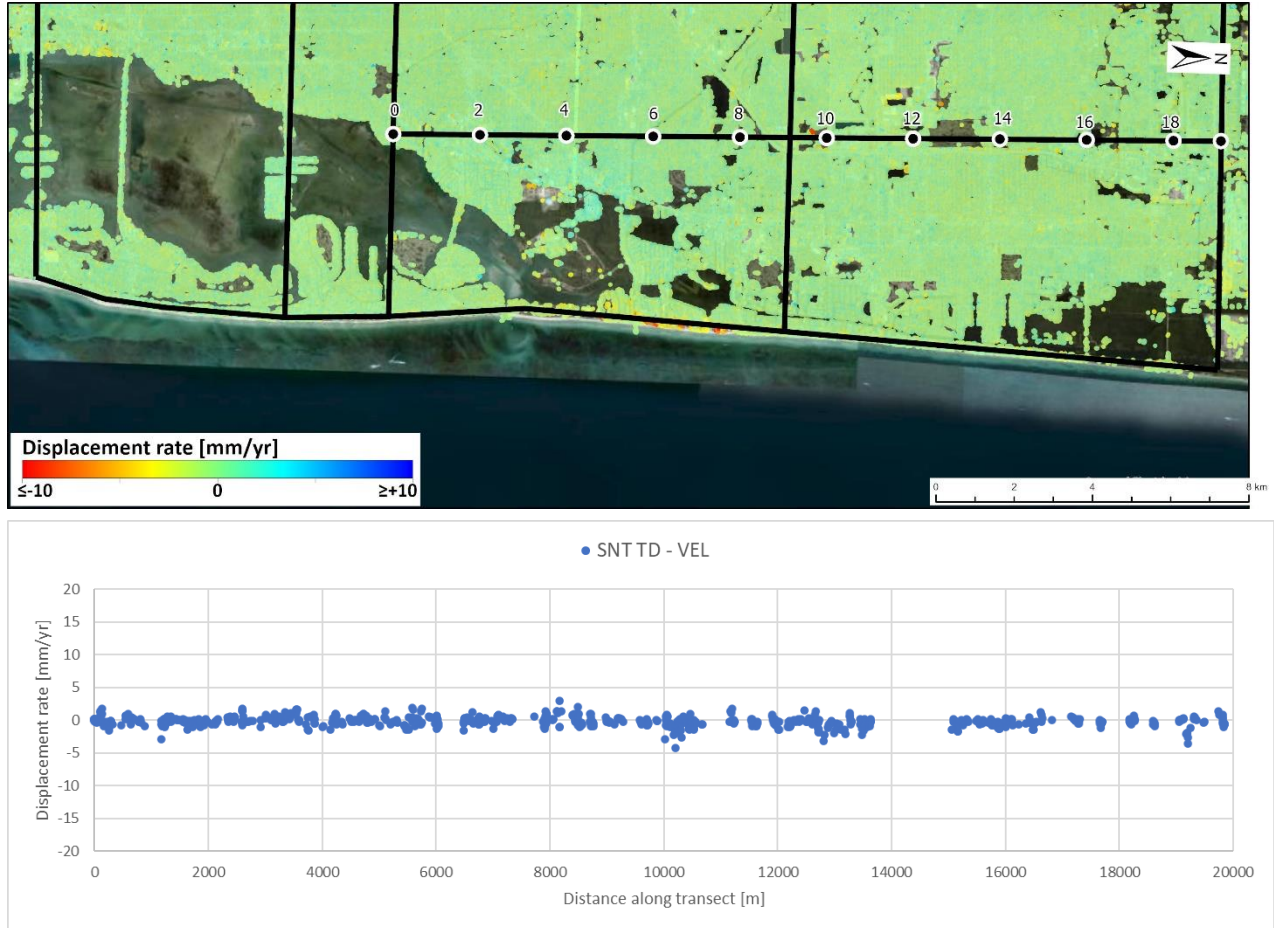
7.7. Local-SNT – TB



7.8. Local-SNT – TC



7.9. Local-SNT – TD



7.10. Local-SNT – TE

